

Article

Interplay of Conformational and Chemical Transformations of ortho-Substituted Aromatic Nitroso Oxides: Experimental and Theoretical Study

Ekaterina Mikhailovna Chainikova, Alfia R. Yusupova, Sergey L. Khursan, Aigul N. Teregulova, Alexander N. Lobov, Marat Faritovich Abdullin, Leniza V. Enikeeva, Irek Marsovich Gubaydullin, and Rustam Lutfulovich Safiullin

J. Org. Chem., **Just Accepted Manuscript** • DOI: 10.1021/acs.joc.7b00537 • Publication Date (Web): 11 Jul 2017

Downloaded from <http://pubs.acs.org> on July 14, 2017

Just Accepted

"Just Accepted" manuscripts have been peer-reviewed and accepted for publication. They are posted online prior to technical editing, formatting for publication and author proofing. The American Chemical Society provides "Just Accepted" as a free service to the research community to expedite the dissemination of scientific material as soon as possible after acceptance. "Just Accepted" manuscripts appear in full in PDF format accompanied by an HTML abstract. "Just Accepted" manuscripts have been fully peer reviewed, but should not be considered the official version of record. They are accessible to all readers and citable by the Digital Object Identifier (DOI®). "Just Accepted" is an optional service offered to authors. Therefore, the "Just Accepted" Web site may not include all articles that will be published in the journal. After a manuscript is technically edited and formatted, it will be removed from the "Just Accepted" Web site and published as an ASAP article. Note that technical editing may introduce minor changes to the manuscript text and/or graphics which could affect content, and all legal disclaimers and ethical guidelines that apply to the journal pertain. ACS cannot be held responsible for errors or consequences arising from the use of information contained in these "Just Accepted" manuscripts.



ACS Publications

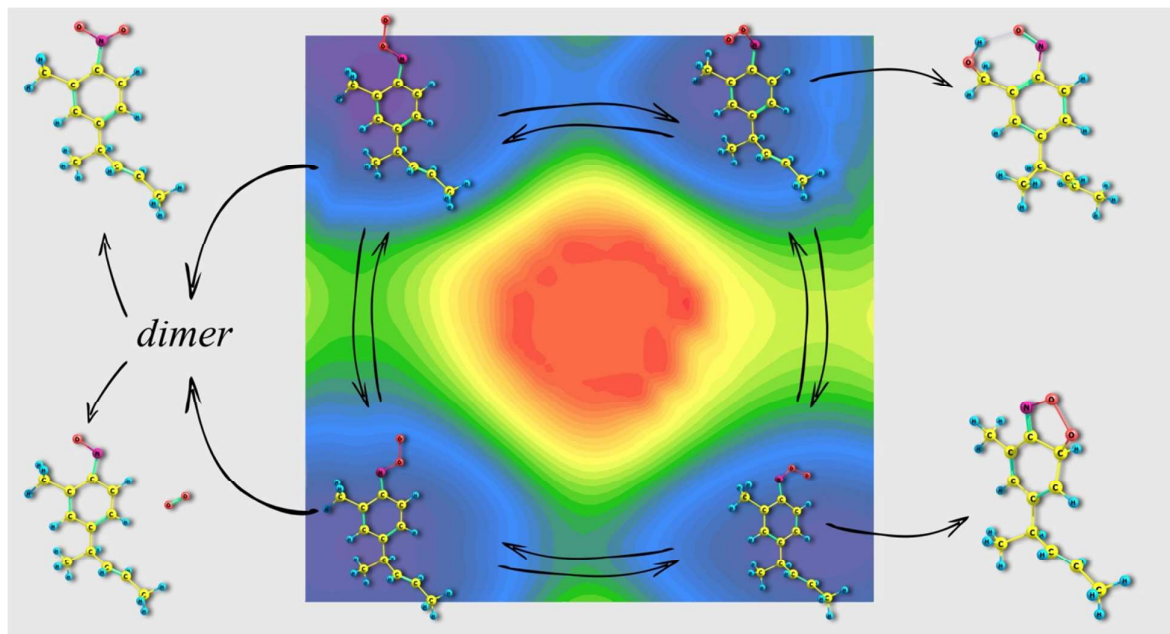
Interplay of Conformational and Chemical Transformations of *ortho*-Substituted Aromatic Nitroso Oxides: Experimental and Theoretical Study

Ekaterina M. Chainikova,^{*,†} Alfia R. Yusupova,[†] Sergey L. Khursan,[†] Aigul N. Teregulova,[†] Alexander N. Lobov,[†] Marat F. Abdullin,[†] Leniza V. Enikeeva,[‡] Irek M. Gubaydullin,[‡] Rustam L. Safiullin[†]

[†]Ufa Institute of Chemistry of the Russian Academy of Sciences, 71 pr. Oktyabrya, Ufa 450054, Russian Federation

[‡]Ufa State Petroleum Technological University, 1 Kosmonavtov St., Ufa 450062, Russian Federation

*E-mail: kinetic@anrb.ru



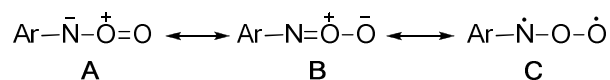
ABSTRACT: The mechanism of the photooxidation of aromatic azides containing a substituent at one of the *ortho* positions (2,4-dimethoxyphenyl azide (**1a**) and 2-methyl-4-[(*2E*)-1-methylbut-2-en-1-yl]phenyl azide (**1b**)) was studied in acetonitrile. The electronic spectra and the kinetic regularities of the consumption of corresponding nitroso oxides, which are the reaction intermediates, were investigated by flash photolysis. Owing to the one-and-a-half order of the C-N and N-O bonds and asymmetric molecule structure these nitroso oxides exist as four conformers (*cis*/*syn*, *cis*/*anti*, *trans*/*syn*, and *trans*/*anti*). The conformers differ in the spectral properties and in the reactivity in various irreversible transformations. The only product – (2*Z*,4*E*)-4-methoxy-6-oxohepta-2,4-dienitrile oxide (**7a**) – was observed during photooxidation of **1a**, whereas transformations of the nitroso oxide isomers derived from **1b** led to a set of stable products: the *cis*/*anti* isomer was transformed into (3,4,7-trimethyl-3a,4-dihydro-2,1-benzisoxazol-5(3*H*)-ylidene)ethanal (**10**), the *trans* isomers recombined forming the corresponding nitro and nitroso compounds, and the most reactive *cis*/*syn* isomer was transformed into *ortho*-nitrosobenzyl alcohol **11**. The last was oxidized slowly to the corresponding benzaldehyde **12**. Interaction of **11** and **12** led to the formation of (*Z*)-1,2-bis(2-formyl-4-((*2E*)-1-methylbut-2-en-1-yl)phenyl)diazene-1-oxide (**13**). The DFT simulation and kinetic modeling of the nitroso oxides transformations as well as the product analysis allowed revealing the fine details of the mechanism of decay for these species.

INTRODUCTION

Aromatic nitroso oxides (ArNOO) are formed by the reaction of nitrenes in their ground triplet state with molecular oxygen.^{1–4} ArNOO have been characterized by matrix isolation spectroscopy.^{5–9} A unique feature of these labile species is their *cis*-*trans* isomerism because of

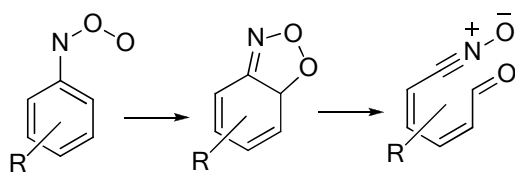
the N–O bond order of ~ 1.5 .^{8,10} Nitroso oxides have a singlet ground state¹¹ and their electronic structure may be described by superposition of main resonances A–C^{4,12} (Chart 1).

Chart 1



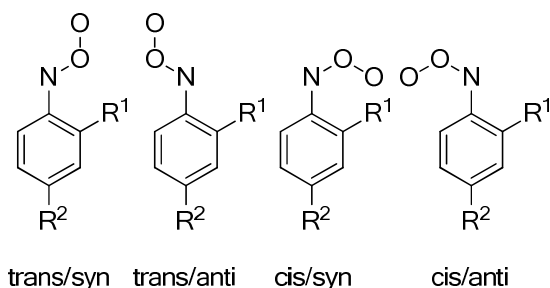
The isomer forms of nitroso oxides differ from each other not only in spectral properties but also in reactivity both in the decay reaction¹³⁻¹⁵ and in reactions with oxidizable substrates.¹⁶ A consumption of most nitroso oxides studied is carried out by first-order reactions¹³ and in the case of the trans isomer is the transformation to the cis isomer, which undergoes a nontrivial redox isomerization via an aromatic ring opening to form diene nitrile oxide (Scheme 1).^{14,15}

Scheme 1. Transformations of the cis Form of Phenylnitroso Oxides



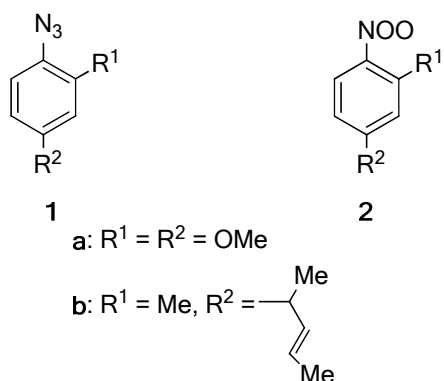
Nitrile oxide, which is formed from 4-methoxyphenylnitroso oxide, was isolated and identified by spectral methods.¹⁴ If the molecule of a parent nitroso oxide possesses a reactive center suitable for the intramolecular addition of the CNO group then corresponding hetero- and carbocyclic compounds are products of a chain of transformations.^{15,17} The presence of a substituent at one of the ortho positions of aromatic nitroso oxide leads to doubling the number of the isomeric forms of the species (Chart 2) and two isomeric products of their transformations should be formed as a result.

Chart 2. Conformers of *ortho*-Substituted Phenylnitroso Oxides



In this work, the mechanism of transformations of *ortho*-substituted nitroso oxides (**2**) which are formed under photolysis of 2,4-dimethoxyphenyl azide (**1a**) and 2-methyl-4-[(2*E*)-1-methylbut-2-en-1-yl]phenyl azide (**1b**) in the presence of oxygen has been studied by experimental and theoretical methods. By flash photolysis, the electronic spectra of the isomeric forms of nitroso oxides **2** were obtained, and the kinetic regularities of their consumption were

studied in acetonitrile. Analysis of the products of the photooxidation of azides **1**, theoretical modeling of elementary stages, as well as kinetic modeling of the process of the decay of nitroso oxides **2** allowed revealing fine details of the reaction mechanism.



Flash Photolysis. Under flash photolysis the azide **1a** solution in acetonitrile in the presence of O_2 a transient absorption, lifetime of which depends on the detection wavelength, was observed in the 350–570 nm range (Figure 1). In the short-wavelength region of this range (350–440 nm), the kinetic curves of the absorption decay were described by a first-order equation (1) (Figure 1a, Curve 1) with the rate constant of $0.14 \pm 0.01 \text{ s}^{-1}$ at room temperature.

$$A = A_{\infty} + A_0 e^{-kt} \quad (1)$$

where A_0 and A_{∞} are optical densities of the solution immediately after excitation and at the end of the reaction, respectively. At wavelengths of 420–480 nm, in millisecond interval, the kinetic curves were recorded (Figure 1a, Curve 2), which also were described by eq 1; the rate constant equals to $(3.1 \pm 0.1) \times 10^3 \text{ s}^{-1}$. Finally, in the range from 460 to 570 nm, the optical density dependences on time had a bi-exponential character and were described by eq 2 (Figure 1a, Curve 3).

$$A = A_{\infty} + A_0^I e^{-k_I t} + A_0^{II} e^{-k_{II} t} \quad (2)$$

Therefore, in this spectral range, a consumption of two intermediates was observed with somewhat different reactivity; in eq 2 A_0^I , A_0^{II} , k_I , and k_{II} are initial optical densities and rate constants of consumption of two species, respectively, while A_{∞} is an end optical density of solution. The rate constants obtained using this equation equal to $1.63 \pm 0.08 \text{ s}^{-1}$ and $0.77 \pm 0.04 \text{ s}^{-1}$ at room temperature.

Under flash photolysis of oxygen-containing solutions of azide **1b** in acetonitrile, the formation of several species was also observed. The most labile of them absorbs in the wavelength range of 360–460 nm and had a lifetime of two orders of magnitude smaller than other species. The kinetic curves of the decay of this intermediate were well described by eq 1. (Figure 1b, Curve 3) with the rate constant of $75 \pm 2 \text{ s}^{-1}$ at room temperature. At wavelengths from 360 to 410 nm, the

absorption decay obeyed a bi-exponential eq 2 (Figure 1b, Curve 1). The rate constants of the consumption of two components were $0.10 \pm 0.01 \text{ s}^{-1}$ and $0.50 \pm 0.01 \text{ s}^{-1}$. In the long-wavelength range ($\lambda > 410 \text{ nm}$) kinetic curves, treatment of which by eq 1 gives the rate constant of $0.50 \pm 0.01 \text{ s}^{-1}$, were recorded (Figure 1b, Curve 3). Therefore, under flash photolysis of azide **1b** in the presence of oxygen, the formation of intermediates of three kinds differing from each another by lifetimes and absorption spectra were observed.

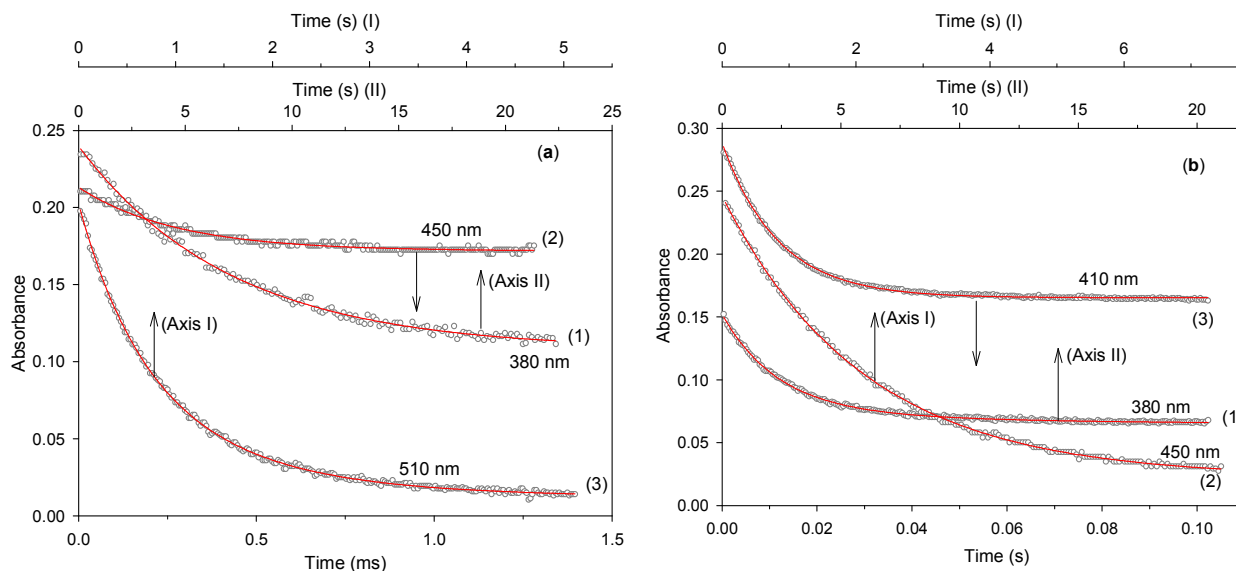


Figure 1. Kinetic traces observed following flash photolysis of azides **1a** (a) and **1b** (b) ($2.5 \times 10^{-4} \text{ M}$) in oxygen-saturated acetonitrile ($T = 295 \text{ K}$). Solid lines correspond to the theoretical description.

The absorption spectra of intermediates of the photooxidation of azides **1a** and **1b** were constructed from the initial optical densities calculated by a treatment of kinetic curves using eqs 1 and 2 (See Supporting Information, Figures S1 and S2 on transient absorption complete spectra at several time). The maxima of these spectra for the most stable species (denote it by the letter **A**) correspond to $\sim 380 \text{ nm}$ in both cases (Figure 2). The absorption maxima of the most labile species (**B**) are around 450 and 410 nm in the cases of azides **1a** and **1b**, respectively (Figure 2). Two remaining intermediates of the photooxidation of azide **1a**, with close reactivity, absorb a light in the long-wavelength range with maxima at $\sim 490 \text{ nm}$ (species **C**) and $\sim 510 \text{ nm}$ (species **D**) (Figure 2a). Analogous intermediates of the azide **1b** photooxidation are apparently consumed with similar rate constants, and their total absorption spectrum has a maximum at the wavelength of $\sim 440 \text{ nm}$ (Figure 2b). It should be noted that the residual optical density on the kinetic curves of the consumption of the most reactive intermediates **B**, lifetimes of which by 2–4 orders of magnitude smaller than lifetimes of the remaining intermediates, equals the sum of

the optical densities of these intermediates at the initial moment in time (Figure 1a, Curve 2; Figure 1b, Curve 3).

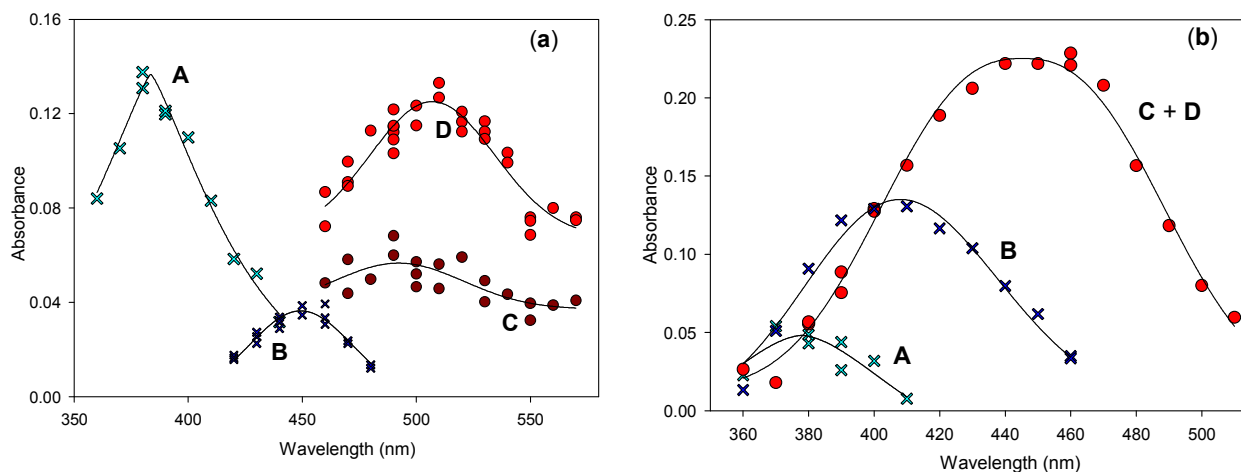


Figure 2. Absorption spectra of species formed following flash photolysis of azides **1a** (a) and **1b** (b) (2.5×10^{-4} M) in oxygen-saturated acetonitrile. T = 295 K.

Table 1. Rate Constants of Decay of Species Formed under Flash Photolysis of Azides **1a** and **1b** in Oxygen-Saturated Acetonitrile [k (s^{-1})] (T = 295 K)

ArN ₃	intermediate			
	A	B	C	D
1a	0.14 ± 0.01	3100 ± 100	1.63 ± 0.08	0.77 ± 0.04
1b	0.10 ± 0.01	75 ± 2	0.50 ± 0.01^a	

^aThe species **C** and **D** are consumed with similar rate constants.

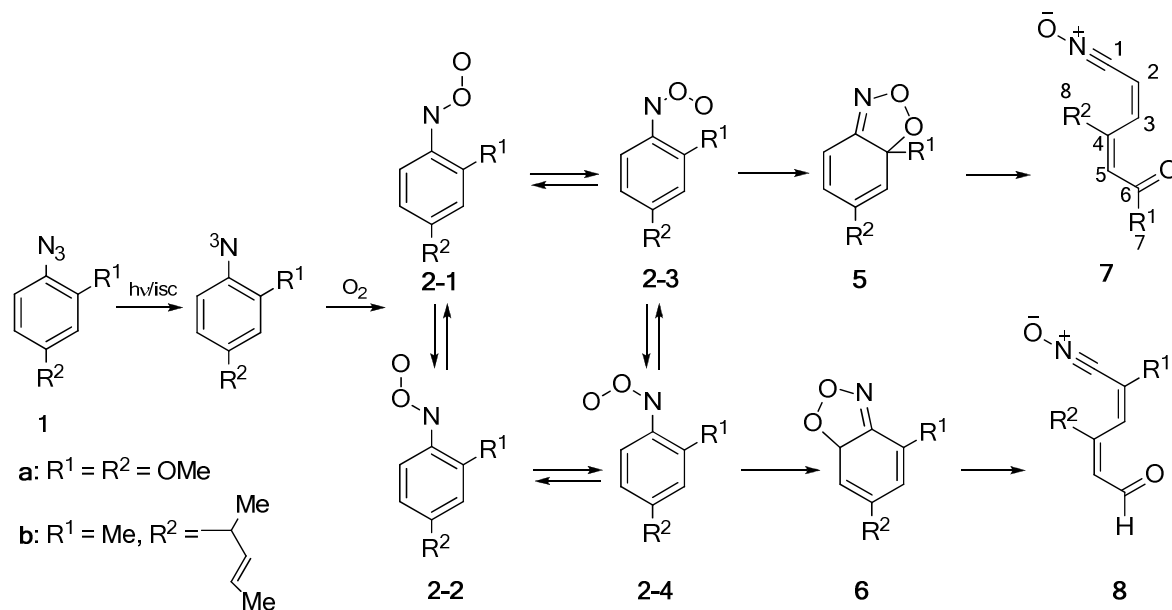
The experimental rate constants of the decay of the species **A–D** are summarized in Table 1.

Previously, in a number of examples, it was shown that aromatic nitroso oxides (phenylnitroso oxide and its *para*-substituted derivatives) absorb in the spectral range from 350 to 650 nm depending on the nature of a substituent and solvent.^{11,13–15,18} Thus, the short-lived absorption observed under flash photolysis of solutions of azides **1** in the presence of oxygen corresponds to nitroso oxides **2a** and **2b**, and the species **A–D** are their isomeric forms shown in Chart 2. The absorption bands will be assigned later.

Products of Azide 1a Photooxidation. Based on the results obtained earlier in the study of the mechanism of the decay of the isomeric forms of aromatic nitroso oxides^{14,15} it was expected that two isomeric nitrile oxides, **7a** and **8a**, should be the end-products of unimolecular transformations of four isomers of nitroso oxide **2a** (Scheme 2). The photolysis of the solution of azide **1a** (6×10^{-4} M) in oxygen-saturated acetonitrile was performed using the filtered light of a xenon lamp ($\lambda = 380\text{--}500$ nm) at 293 K. The progress of the reaction was monitored by reverse-

phase HPLC (See Experimental Section). Judging from the chromatogram of the reaction mixture (See Supporting Information, Figure S1), a single product was formed as a result of the reaction. This was isolated and analyzed. The obtained compound has a molecular weight equal to the molecular weight of nitroso oxide **2a** ($C_8H_9NO_4$) – 183. The IR spectrum exhibits an intense band at 2297 cm^{-1} corresponding to stretching vibrations of the $C\equiv N$ bond. Analysis of the NMR spectra (1H and ^{13}C) allowed the conclusion to be drawn that the obtained product is (2*Z*,4*E*)-4-methoxy-6-oxohepta-2,4-dienenitrile oxide (**7a**) (yield to azide consumed was 94%) (See Experimental Section and Supporting Information). Thus, only the *cis/syn* form of nitroso oxide **2a** (structure **2a-3** in Scheme 2) is transformed to the end-product of the reaction.

Scheme 2. Proposed Mechanism for Photooxidation of Azides 1

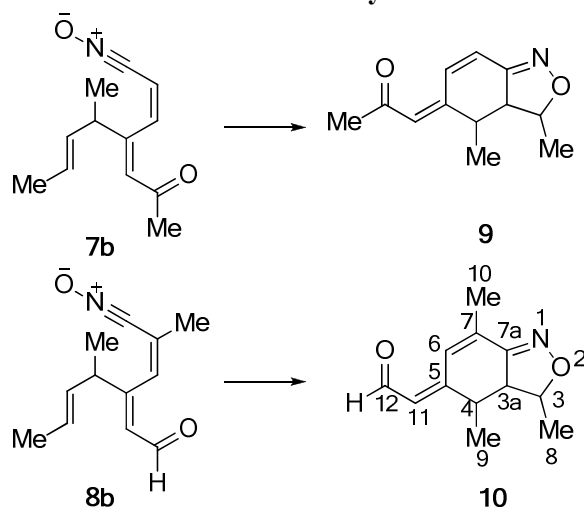


Products of Azide 1b Photooxidation. It was expected that the chain of unimolecular transformations of nitroso oxide **2b** should lead to the formation of nitrile oxides **7b** and **8b** (Scheme 2). In this case, the proposed reaction mechanism is supplemented by the stage of the intramolecular [3+2]-cycloaddition of the nitrile oxide group to the double bond of the allyl fragment to form benzisoxazoles **9** and **10**^{15,19,20} (Scheme 3).

The azide **1b** photooxidation in acetonitrile led to a complicated mixture of products (Figure 3a). During standing of the obtained reaction mixture in the dark at room temperature, the signal of a product with the retention time $t_R = 3.8$ min decreased and finally disappeared (Figure 3b). It was accompanied initially by growth then decreasing and full disappearance of the signal of a product with $t_R = 4.5$ min and by growth of the signal at $t_R = 7.1$ min. This process was continued for about 72 hours. The signals with the retention times of 3.3, 5.2, and 5.9 min were not changed (Figure 3). Thus, obviously the mechanism of the azide **1b** photooxidation is

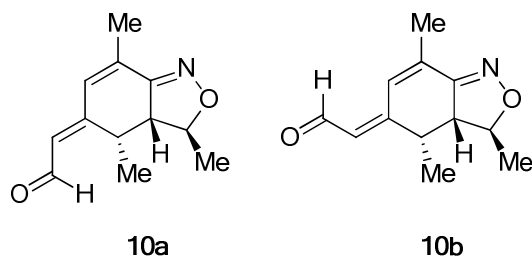
more complicated than that presented in Schemes 2 and 3. One can make a preliminary conclusion that the reaction leads to stable products with the retention times of 3.3, 5.2 and 5.9 min as well as to a labile product with the retention time of 3.8 min which is transformed via an intermediate with the retention time of 4.5 min into an end-product with the retention time of 7.1 min. A chromatographic separation of the reaction mixture was performed immediately after stopping of the reaction to isolate intermediates ($t_R = 3.8$ and 4.5 min) and after standing of the reaction mixture in the dark at room temperature for 72 hours to isolate stable products ($t_R = 3.3$, 5.2, 5.9, and 7.1 min). Identification of the obtained products was achieved using APCI-MS and ^1H and ^{13}C NMR spectroscopy (See Experimental Section and Supporting Information).

Scheme 3. Intramolecular Cyclization of Nitrile Oxides



The molecular weight of the product with the retention time of 3.3 min is 205, which equals the molecular mass of nitroso oxide **2b** ($\text{C}_{12}\text{H}_{15}\text{NO}_2$). According to NMR data, this is (3,4,7-trimethyl-3a,4-dihydro-2,1-benzisoxazol-5(3*H*)-ylidene)ethanal (**10**, Scheme 3). Benzisoxasole **10** is formed from the cis/anti form of nitroso oxide **2b** according to Schemes 2 and 3 as a mixture of two isomers **10a** and **10b** (ratio of about 2:1) (Chart 3), which differ by the aldehyde group position with respect to the double bond.

Chart 3. Isomers of Benzisoxasole 10



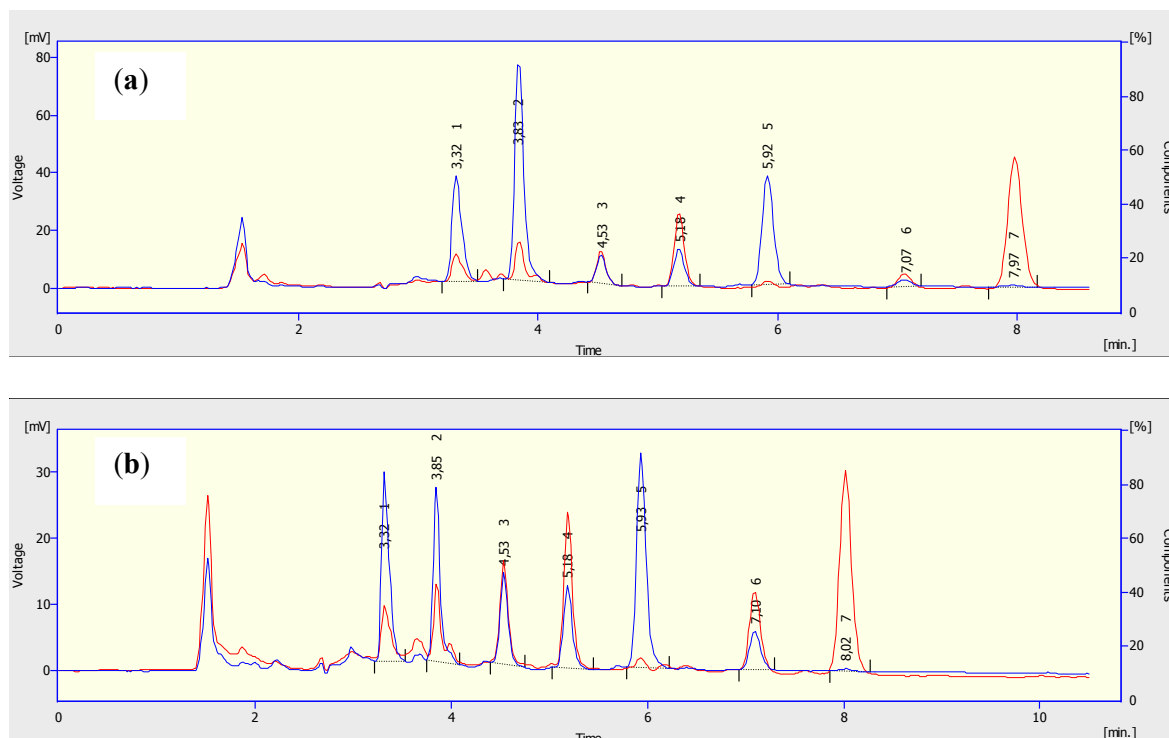
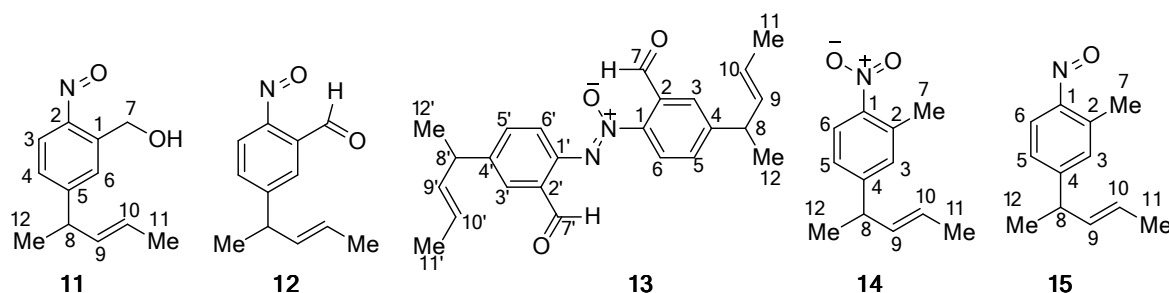


Figure 3. Chromatograms of the reaction mixture obtained by photolysis of an oxygen-saturated acetonitrile solution of azide **1b** (5×10^{-4} M) at 293 K. The mobile phase was acetonitrile–water (92:8), and the detection wavelengths were 250 and 320 nm. After stopping the reaction (a) and standing this reaction mixture in the dark for ~36 hours (b). $t_R = 8.0$ min (azide **1b**). See text for details.

The molecular weight of a labile product with $t_R = 3.8$ min also equals the molecular mass of nitroso oxide **2b** (205). The NMR spectra of this compound confirm that the aromatic ring and allyl substituent were not affected during the reaction and that its molecule contains a methylene group. Thus, we came to the conclusion that this product is {5-[(2*E*)-1-methylbut-2-en-1-yl]-2-nitrosophenyl}methanol (**11**) (Chart 4), which was evidently formed from the cis/syn form of nitroso oxide **2b**.

Chart 4. Products of Photooxidation of Azide **1b**

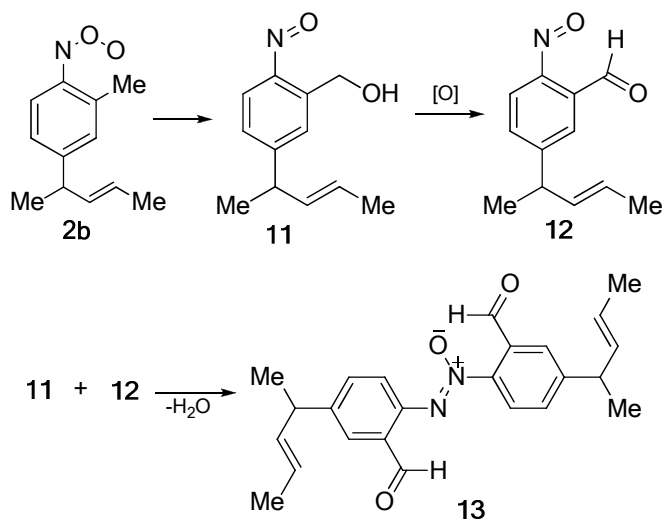


A product with $t_R = 4.5$ min, which judging from chromatograms was formed from nitrosobenzyl alcohol **11**, was not obtained in quantities sufficient for NMR analysis. However,

we were able to measure its molecular weight which is 203, i.e. the molecular mass of nitroso oxide **2b** minus the mass of two protons. Based on this, we concluded that this intermediate of the photooxidation of azide **1b** is 5-[(2*E*)-1-methylbut-2-en-1-yl]-2-nitrosobenzaldehyde (**12**) (Chart 4).

The molecular weight of a compound with $t_R = 7.1$ min, which was formed as the products **11** and **12** were being consumed (Figure 3), is 390, which equals the sum the molecular mass of **11** and **12** minus the molecular mass of H_2O : $205 + 203 - 18 = 390$. The 1H NMR spectrum contains nine signal groups including the aldehyde ones. In each group, the signals are paired and have the same intensity. The same was observed in the ^{13}C NMR spectrum, which contains twelve groups of paired signals (See Experimental Section and Supporting Information). This confirms that a molecule has two identical fragments connected by a nonsymmetrical bridge. Analysis of the obtained results allowed the conclusion to be drawn that this compound is (*Z*)-1,2-bis(2-formyl-4-[(2*E*)-1-methylbut-2-en-1-yl]phenyl)diazene-1-oxide (**13**) (Chart 4). On the basis of the above, we can offer a formal scheme for the formation of azoxy compound **13** from nitroso oxide **2b** (Scheme 4). According to this scheme, an initial intramolecular redox isomerization of the *cis/syn* form of nitroso oxide **2b** into nitrosobenzyl alcohol **11** occurs. A more detailed analysis of the proposed scheme with the using of quantum-chemical modeling methods is presented below.

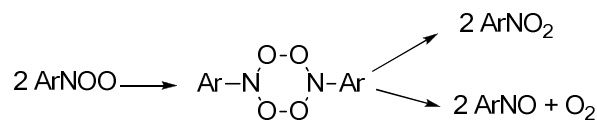
Scheme 4. Proposed Scheme of the Transformation of the *cis/syn* Form of Nitroso Oxide **2b into the Final product **13****



The molecular weights of products with the retention times of 5.2 and 5.9 min (Figure 3) are 205 and 189. Based on the NMR data, they were identified as 2-methyl-4-[(2*E*)-1-methylbut-2-en-1-yl]-1-nitrobenzene (**14**) and 2-methyl-4-[(2*E*)-1-methylbut-2-en-1-yl]-1-nitrosobenzene (**15**) (Chart 4).

Simultaneous formation of nitro and nitroso compounds upon the photooxidation of aromatic azides was explained by the bimolecular reaction of nitroso oxides^{11,17,18} (Scheme 5).

Scheme 5. Bimolecular Reaction of Nitroso Oxides to Form Nitro and Nitroso Compounds



Thus, analysis of the products of the azide **1b** photooxidation leads to the conclusion that the mechanism of the decay reaction of the isomeric forms of nitroso oxide **2b** is more complex than might be expected based on Schemes 2 and 3. Three channels of the consumption of this species have been revealed: (i) the isomerization of the *cis/anti* form into benzisoxazole **10**, (ii) the isomerization of the *cis/syn* form into nitrosobenzyl alcohol **11**, and (iii) the bimolecular decay reaction in which all four isomeric forms could participate.

To compare the obtained results with those of the kinetic studies, the yields of the products **10**, **11**, **14**, and **15**, which were formed upon flash photolysis of azide **1b** in the presence of oxygen, were measured by HPLC using the calibration plots (Table 2).

Table 2. Yields of Products of the Transformations of Nitroso Oxide **2b upon Flash Photolysis of Azide **1b** in Oxygen-Saturated Acetonitrile at Different Temperatures^a**

[1b] ₀ × 10 ⁵ (M)	T (K)	Δ[1b] × 10 ⁵ (M)	[product] × 10 ⁵ (M)			
			10	11	14	15
9.7	333	1.75	0.41 {23} (29)	0.82 {47} (58)	0.10 {4} (6)	0.08 {6} (7)
10.6	293	1.88	0.23 {12} (16)	0.97 {52} (69)	0.12 {4} (6)	0.08 {6} (9)
10.6	264	1.58	0.07 {4} (8)	0.57 {36} (65)	0.07 {4} (8)	0.17 {11} (19)
10.6	253	1.12	0.07 {6} (8)	0.53 {47} (61)	0.10 {9} (11)	0.17 {15} (20)
10.7	251	1.34	0.06 {4} (7)	0.54 {40} (63)	0.08 {6} (9)	0.17 {13} (21)

^aThe solution of azide was irradiated by six light pulses. In curly brackets yields (%) on azide consumed; in parentheses the part of the product (%) in a sum of products **10**, **11**, **14**, and **15**.

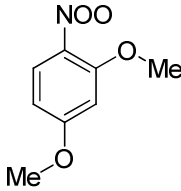
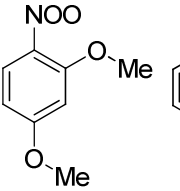
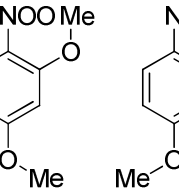
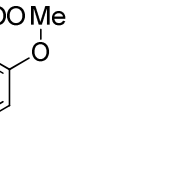
As seen from this Table, nitrosobenzyl alcohol **11** (Chart 4), which formed from the *cis/syn* form of nitroso oxide **2b**, was the main product of the consumption of this species. Its yield varies little with decreasing temperature from 293 to 251 K. In this temperature interval, the percentage of benzisoxazole **10**, a product of the isomerization of the *cis/anti-2b* (Schemes 2, 3), decreases by about twice, and the total yield of products **14** and **15** resulting from the

bimolecular reaction of nitroso oxides, conversely, increases in the same proportion. Increasing the temperature from 293 to 333 K led to a reduction of the alcohol **11** yield by 11%, the growth of the benzisoxazole **10** that by 13%, and a very small decrease of the total yield (2%) of the nitro and nitroso compounds **14** and **15**.

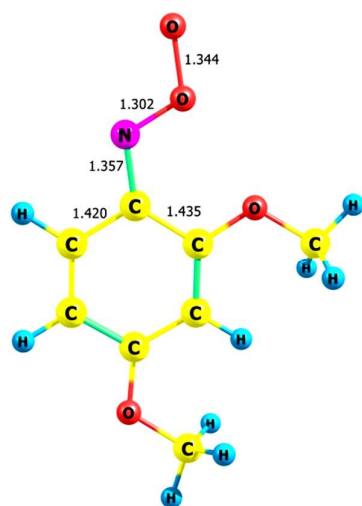
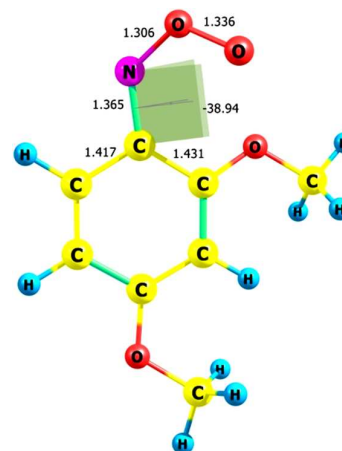
DISCUSSION

Geometries and energies. To explain the obtained results, DFT calculations were performed for all conformers of nitroso oxides **2a** and **2b** (**2-1–2-4**, Scheme 2) as well as for the primary products **5** and **6** (Scheme 2) of unimolecular decay of these species. In the **2a** molecule, besides the rotation of the nitroso oxide moiety around the N–O and C–N bonds determining the existing of four conformers, a free rotation of ortho and para methoxy substituents around the C–O bonds occurs. The optimal orientations of both methoxy groups were found using *cis/syn* isomer of 2,4-dimethoxyphenyl nitroso oxide as a testing molecule (Chart 5, Structure **II**) and were used when studying conformational transformations of **2a** around N–O and O–O bonds. The search for the optimal orientation of the substituents in nitroso oxide **2b** was performed in the same way.

Chart 5. Standard Enthalpies and Gibbs Energies of the Conformers of *cis/syn*-2,4-Dimethoxyphenyl Nitroso Oxide.

				
	I	II	III	IV
ΔH° (kJ/mol)	2.2	0.0	14.1	11.8
ΔG° (kJ/mol)	7.1	0.0	20.6	19.2

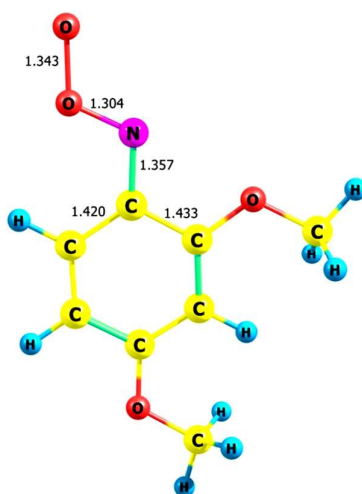
The structures of all conformers of **2a** are displayed in Figure 4. The deviation from the planarity of the nitroso oxide moiety relative to the 6π aromatic system due to a steric repulsion between the NOO group and the methoxy substituent at the ortho position is a structural feature of the *cis/syn* isomer **2a-3**. In other cases, the planarity of the NOO fragment is preserved. It was found that the *cis* and *trans* states of **2a** have a close energies, which is consistent with the results reported in the work of ref 21 for a number of *para*- and *ortho*-substituted phenylnitroso oxides.

**2a-2****2a-3** ΔH° (kJ/mol) 5.1

20.7

 ΔG° (kJ/mol) 6.0

22.6

**2a-1** ΔH° (kJ/mol) 3.0

0.0

 ΔG° (kJ/mol) 3.5

0.0

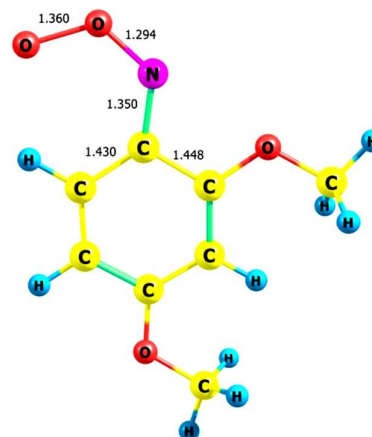
**2a-4**

Figure 4. Stable conformers of nitroso oxide **2a**. The standard enthalpies and Gibbs energies of conformers with respect to **2a-4** are presented. Bond distances in angstroms and bond angles in degree.

The cis/anti isomer **2a-4** is most stable conformer of **2a** and the structure **2a-3** is most labile, which undoubtedly is connected to the steric effect. The structural features and relative energies of the conformers of nitroso oxide **2b** in the main are similar to those of nitroso oxide **2a**. The only important difference is the highest thermodynamic stability of the trans/anti isomer **2b-1**,

although the relative energy of the cis and trans forms, as for other nitroso oxides, do not differ very much. The presence of the ortho methyl group in nitroso oxide **2b** leads to even greater deviation from the planarity of the NOO group in the cis/syn isomer **2b-3** (45.4 degrees) than in **2a-3** (Figure 4). Therefore, the cis/syn isomer **2b-3** is also most labile ($\Delta G^\circ = 22.4$ kJ/mol). Geometric parameters, absolute enthalpies, and Gibbs free energies of all compounds and transition states studied are presented in Supporting Information.

Formation of Products. The theoretical modeling of the transformations of two cis forms of nitroso oxide **2a** into corresponding nitrile oxides (Scheme 2) was performed. The Gibbs activation energy of the stage of the formation of the bicycle **5a** from the cis/syn form **2a-3** was 43.1 kJ/mol, whereas the activation barrier of the analogous transformation of *cis/anti-2a* was almost twice as high – 84.7 kJ/mol. Such a large difference in the activation energies of the two possible pathways for the consumption of nitroso oxide **2a** explains why nitrile oxide **7a** was the only product of the azide **1a** photooxidation.

Analogous to **1a**, we expected that benzisoxazole **9**, which is formed from the cis/syn form of nitroso oxide **2b** (Schemes 2, 3), would be the main product of the azide **1b** photooxidation. However, nitrosobenzyl alcohol **11**, as the main product, and benzisoxazol **10**, the precursor of which is nitrile oxide **8b** formed in turn from the cis/anti isomer **2b-4**, were found in the reaction mixture (Table 2). The M06-L/6-311+G(d,p) calculations give the activation barrier of the ortho-cyclization of the cis/anti isomer **2b-4** $\Delta G^\ddagger = 77.1$ kJ/mol. At the same time the analogous transformation of the cis/syn isomer **2b-3** with $\Delta G^\ddagger = 61.2$ kJ/mol was not observed. This result is not associated with an error of the theoretical estimation of the activation barriers using M06-L functional. Indeed, the difference in the activation energies of the ortho-cyclization $\Delta\Delta G^\ddagger = \Delta G^\ddagger(\text{cis/anti}) - \Delta G^\ddagger(\text{cis/syn})$ were re-calculated using mPWPW91 and HCTH density functionals, the applicability of which when describing properties of nitroso oxides was demonstrated in the work of ref 21. In all cases, the $\Delta\Delta G^\ddagger$ values were in the interval from 16 to 19 kJ/mol. This seeming contradiction is explained by the presence of the energetically more favorable in comparison with the ortho-cyclization channel of the consumption of the cis/syn form of nitroso oxide **2b**, namely the direct oxidation of the ortho methyl substituent by the nitroso oxide group to form nitrosobenzyl alcohol **11**. The Gibbs activation energy of this channel calculated using three functionals mentioned above on average by 10 kJ/mol smaller than the activation energy of the ortho-cyclization of the cis/syn isomer **2b-3**, i.e. the competition of two channels of the **2b-3** decay to form **7b** \rightarrow **9** and **11** \rightarrow **12** \rightarrow **13** is in favor of the last: the ratio of the reaction rates w_{11}/w_{7b} is about 60 (295 K). It should be noted that such intramolecular oxidation of an ortho substituent by the NOO group is new type of rearrangement of aromatic

nitroso oxides which was found for the first time in this work. The theoretical modeling of the process of the formation of the compound **11** was performed in the M06-L/6-311+G(d,p) approximation and is illustrated in Figure 5. The first stage of this mechanism is the abstraction of the H atom from the ortho methyl substituent by the terminal oxygen atom of the nitroso oxide group of the cis/syn isomer of **2b**. Favorable conditions for the occurrence of this transformation are the spatial proximity of the reaction centers, a high chemical potential of nitroso oxide, and reduced strength of the C–H bond owing to the possibility of stabilization of the intermediate formed due to the restructuring of the π system of the molecule. It was found that the activation enthalpy of the H atom abstraction was 48.2 kJ/mol.

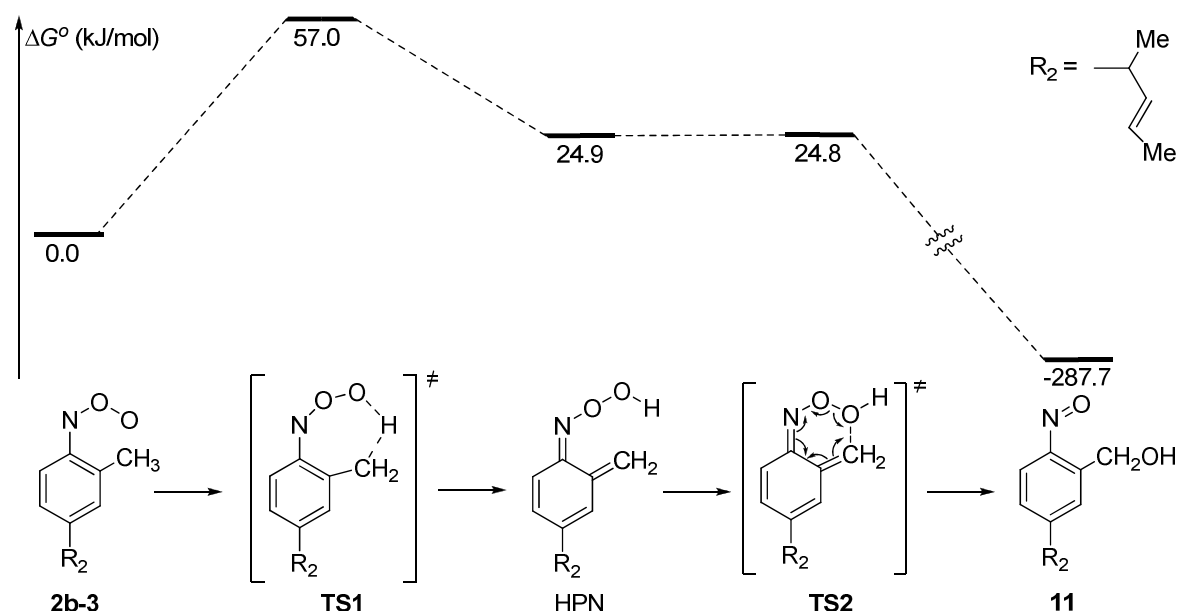
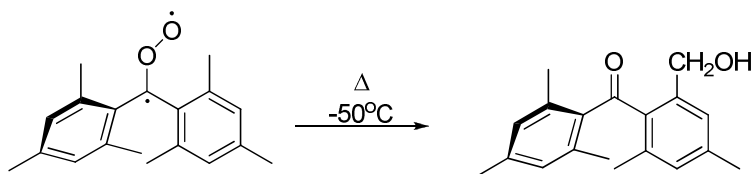


Figure 5. Energetic diagram of the compound **11** formation. Calculation by the M06-L/6-311+G(d,p) + IEFPCM approximation.

The product of the H atom abstraction is the syn isomer of hydroperoxynitrene (**HPN**), which possesses a chain of three electronegative atoms bonded to each other by an ordinary covalent bond, =N–O–O. Heterocyclic compounds containing such structural fragment were discussed by authors of ref 22. The conformational rotation around the O–O bond and the formation of the thermodynamically more favorable anti form of **HPN** is accompanied by overcoming a small activation barrier (**TS2** in Figure 6, $\Delta H^\ddagger = 1.1$ kJ/mol, calculation for gas phase) and by substantial elongation of the peroxide bond (1.573 Å). A test of a stability of the anti isomer wave function indicates a significant spin polarization in the molecule. However, the re-optimization of the structure of the anti form of **HPN** with account of the non-equivalence of α and β electron systems led immediately to nitrosobenzyl alcohol **11**. Thus, the activation barrier of the conformational transformation of hydroperoxynitrene **TS2** is essentially the one of the isomerization of **HPN** into **11**. The account of solvation effects decreases the value of this barrier

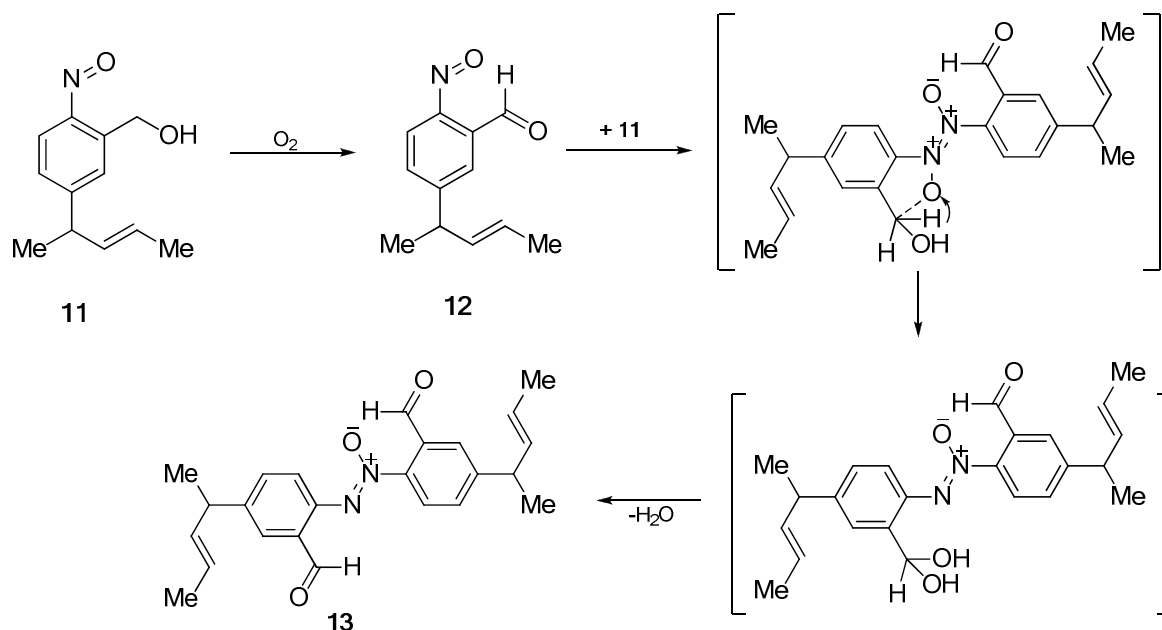
up to zero (Figure 5). Generally, the results of the theoretical modeling of the new isomerization reaction of aromatic nitroso oxides are consistent with the preferable formation of nitrosobenzyl alcohol **11** and testify that the limiting stage of this reaction is the intramolecular abstraction of the H atom in **2b-3**, and the subsequent rapid transformation of **HPN** into the stable product **11** occur by the intramolecular hydroxylation of the methylene group. It is worth to note the found new reaction of ArNOO is consistent with known chemical behavior of 1,3-dipolar species family which includes ozone, carbonyl oxides, and nitroso oxides. The H atom abstraction with ozone is known to be the initiation step of free-radical oxidation of organic substances by $O_3 - O_2$ or $O_3 - N_2$ gas mixtures.^{23,24} The direct analogy with found transformation of **2b** was observed earlier for aromatic carbonyl oxides as well. Dimesitylketone O-oxide was obtained in the $CFCl_3 - (CF_2Br)_2$ glassy matrix at 77 K by irradiation of corresponding diazocompound in the presence of oxygen. Warming to room temperature resulted in the disappearance of carbonyl oxide and the formation of 2-(hydroxymethyl)-4,6-dimethylphenyl mesityl ketone as the main product:²⁵



It is obvious, the observed similarity in chemical properties of 1,3-dipoles is caused to its partially biradical character as it is shown in Chart 1 (resonance C).

The formation of azoxycompound **13** occurs more likely from nitrosobenzyl alcohol **11** via reactions being typical for nitroso compounds. We can assume that during prolonged standing of the reaction mixture, alcohol **11** was oxidized with oxygen to aldehyde **12**. Indeed, using a high-precision volumetry setup, we have showed that the reaction mixture obtained by photooxidation of azide **1b**, when standing, is absorbing oxygen in a stoichiometric ratio of 1:1, based on alcohol **11** consumed (See Supporting Information for details). It is well known that the characteristic feature of nitroso groups bonded to a carbon atom is their ability to dimerize.²⁶ An interaction of alcohol **11** with aldehyde **12** gives the mixed dimer (Scheme 6), which loses the water molecule to form the final product **13**.

Scheme 6. Proposed Mechanism for the Formation of Azoxy Compound 13



Spectral properties and identification of isomers. Obviously, the above-described spectral detection of several species formed upon photolysis of the solutions of azides **1** in the presence of oxygen is due to the existence of conformers of nitroso oxides **2** (Scheme 2). To assign an observed absorbance to the particular structure, the electronic spectra of the conformers were calculated using the TD-DFT method. The spectral characteristics of the long-wavelength S–S transitions with maximal oscillator forces (f_{osc}) are shown in Table 3.

The results of theoretical calculations of the electronic spectra are in reasonable agreement with the observed spectral picture (Figure 2); therefore, establishing of the correspondence between the experimental spectra and conformers of nitroso oxides does not cause difficulties. Consider the assignments of the observed spectral bands to the particular isomers on the example of nitroso oxide **2a**. Previously, it was found that maxima of the absorption spectra of the *cis* isomers of *para*-substituted phenylnitroso oxides are blue-shifted in compare to those of the *trans* isomers.¹³ Therefore, it can be argued that the species **A**, the absorption maximum of which is about 380 nm (Figure 2a), is the *cis*/*anti* isomer **2a-4**. In addition, this isomer is thermodynamically most stable, which explains the low rate constant of the consumption of the intermediate **A** (Table 1, Figure 1a). On the contrary, species **B**, the absorption spectrum of which is also in the short-wave range with $\lambda_{\text{max}} \sim 450$ nm (Figure 2a), was consumed faster than the other and corresponds to the activated by a steric interaction *cis*/*syn* isomer **2a-3**. It is important to note that the TD-DFT calculations of the spectral properties of the *cis* isomers are in good agreement with experimental data both in the λ_{max} position and in the observed bathochromic shift of the absorption maximum of **2a-3** (Table 3).

Table 3. TD-DFT Modeling of Electron Spectra of Conformers of Nitroso Oxides 2^a

conformer	M06-L		mPWPW91		CAM-B3LYP		exp
	λ_{max} (nm)	f_{osc}	λ_{max} (nm)	f_{osc}	λ_{max} (nm)	f_{osc}	λ_{max} (nm)
2a							
2-1 (trans/syn)	386	0.368	424	0.568	407	0.561	490
2-2 (trans/anti)	407	0.302	453	0.500	431	0.574	510
2-3 (cis/syn)	403	0.214	438	0.263	398	0.240	450
2-4 (cis/anti)	361	0.385	393	0.441	380	0.469	380
2b							
2-1 (trans/syn)	384	0.590	409	0.585	386	0.626	440
2-2 (trans/anti)	403	0.549	429	0.531	403	0.623	440
2-3 (cis/syn)	406	0.228	432	0.222	392	0.196	410
2-4 (cis/anti)	359	0.465	381	0.462	363	0.433	380

^aCalculation by the DFT/6-311+G(d, p) + IEFPCM approximation, f_{osc} is oscillator force.

The intermediates **C** and **D**, which slightly differed from each another in the absorption spectra (Figure 2a) and had a moderate reactivity (Table 1), were assigned to the trans/syn (**C**) and trans/anti (**D**) isomers of nitroso oxide **2a**. The estimations of the thermodynamic stabilities of the trans isomers of **2a** (Figure 4) do not contradict such assignment. The TD-DFT calculations for **2a-1** and **2a-2** overestimate an electron transition energy and, accordingly, underestimate the value of λ_{max} . A similar pattern in the calculation of the electronic spectra of nitroso oxides was also noted previously.¹⁰ The reason for the observed deviations is currently unclear. We note only that the use of other density functionals and complication of the basis set, an explicit account of solvation effect by the supermolecule method, did not improve the situation in a meaningful way. Yet another result that deserves attention is the significant decrease in the oscillator force of the S-S transition in the cis/syn isomer (Table 3). The reason for this effect is a deviation from the planarity in the isomer **2a-3** (Figure 4) and a reduction of the conjugation of the nitroso oxide group with the aromatic ring.

A similar assignment of the absorption bands was performed for all isomers of nitroso oxide **2b**; the results are shown in Table 3.

Kinetic modeling. Thus, upon flash photolysis of azides **1** in the presence of oxygen, four isomeric forms of corresponding nitroso oxides **2** were generated. Their consumptions occurred with different rates and led to various products. Nitrile oxide **7a** was the only product of the transformations of nitroso oxide **2a** (Scheme 2), whereas the compounds **10–15** were formed as a result of the consumption of nitroso oxide **2b**. Obviously, the isomers of nitroso oxides undergo mutual conformational transformations; therefore, the measured rate constant of the isomer decay is effective, i.e. it describes a complex of reversible conformational transitions and irreversible transformations into the reaction products. To confirm our ideas, the kinetic modeling of the processes of the decay of nitroso oxides was performed in the framework of the mechanism shown in Scheme 2, which was revised taking into account particularities of the reactivity of each nitroso oxide. All model calculations were carried out for room temperature. The initial concentrations of the conformers were calculated from the experimental values of their initial optical densities using the corresponding oscillator force (Table 3) or were taken to be equal to 2.5×10^{-6} M (the total initial concentration of the conformers was always equal to 10^{-5} M). To calculate initial approximations for rate constants of elementary stages, stable states of all isomers and transition states of all their transformations were localized (See Supporting Information), the absolute values of G° of all states were found, and the Gibbs free activation energies (ΔG^\ddagger) were determined by the M06-L/6-311+G(d,p) method. Initial values of rate constants of elementary stages were calculated by the Eyring equation (3):

$$k = \kappa \frac{k_B T}{h} \exp\left(\frac{-\Delta G^\ddagger}{RT}\right) \quad (3)$$

where κ is Wigner tunneling correction factor that was taken to be 1. After solving the system of the ordinary differential equations (ODE) the kinetic curves of the consumption of the conformers were recovered. From these curves, the effective rate constants k_{eff} were calculated and compared with the experimentally determined those. Then, the set of elementary rate constants k_i was changed by varying the G° values for all conformers and transition states involved in the process of the decay of nitroso oxide, and the ODE system was resolved. The kinetic modeling was continued as long as the value of k_{eff} did not coincide with the experimental rate constant in the range of 1–3%. The solution of the ODE system was performed in the framework of the one-stage second-order Rosenbrock scheme using the Matlab R2014a computing environment. The genetic algorithm, which has worked well in solving the chemical kinetics problems,²⁷ was chosen as optimization method.

The case of 2a. The ODE system corresponds to Scheme 7, at that the intramolecular cyclization of the cis/syn isomer **2a-3** to form the intermediate **5a** ($\Delta G^\ddagger = 43.1$ kJ/mol), which is quickly transformed into the end-product **7a**, is the only irreversible channel of the **2a**

consumption. Preliminary calculations have shown that the ortho-cyclization of the *cis*/*anti* isomer **2a-4** requires much more energy: $\Delta G^\ddagger = 84.7$ kJ/mol. Therefore, the probability of the formation of intermediate **6a**, and consequently nitrile oxide **8a**, is extremely small (Scheme 2). These results explain the fact that in the experiment, only nitrile oxide **7a** was found to be a product of the azide **1a** photooxidation. Therefore, during the kinetic modeling of Scheme 7, the alternative channel of the nitroso oxide **2a** consumption was ignored, believing $k_{46} = 0$. We note that such a pronounced differentiation of the direction of the intramolecular cyclization of nitroso oxides is in full agreement with the results in ref 28, where it was established that the presence of the methoxy substituent at the attacked ortho position noticeably reduces the activation barrier of the ortho-cyclization of nitroso oxide. This paradoxical at first glance an effect is explained by the steric repulsion of the substituents which distorts the planar structure of nitroso oxide, making its geometry closer to the transition state of the ortho-cyclization (Figure 4).

The solution of the system of five differential equations with nine kinetic constants (four pairs of conformational transformations plus the irreversible consumption of **2a-3**, Scheme 7) was conducted with different initial conditions. The total initial concentration of **2a** was 10^{-5} M, and the initial distribution of the isomers **2a-1–2a-4** (0.30:0.18:0.34:0.17, respectively) was estimated from the initial optical densities (Figure 2a) and values of f_{osc} (Table 3), which are proportional to the extinction coefficients of the isomers. Furthermore, the calculation was conducted with an equimolar distribution of the isomers because the rate constants of the reaction of molecular oxygen with triplet nitrenes to form the *cis* and *trans* nitroso oxides are apparently close. A closeness of the rate constants of the formation of *cis*- and *trans*-HNOO was marked previously on the example of the imidogene oxidation.²⁹ The results of kinetic modeling showed a negligible effect of the initial conditions to the main kinetic regularities of the process under study. The optimal values of the Gibbs free energies and corresponding values of ΔG° and ΔG^\ddagger , as well as the rate constants of the elementary stages of the reaction, were found. Calculated time dependencies of concentrations of all participants of the process (See Supporting Information) correspond to the effective rate constants of the consumptions of all isomers of **2a** (Table 4).

Chemical reaction scheme showing the interconversion of various 3,5-dimethoxyphenyl isomers and their derivatives. The scheme includes structures 2a-1, 2a-2, 2a-3, 5a, 6a, and 7a, with equilibrium and reaction arrows labeled with rate constants k_{12} , k_{14} , k_{21} , k_{32} , k_{34} , k_{35} , k_{41} , k_{43} , k_{46} , and k_{48} .

20

Table 4. Results of Kinetic Modeling of Decay of Nitroso Oxides 2^a

transformation	ΔG°	ΔG^\ddagger	k_+^b	k_-^b	$k_{\text{eff}}^{c,d}$	exp ^e
2a						
2a-1 \rightleftharpoons 2a-2	-0.4	70.8	2.4	2.1	0.77	0.77
2a-2 \rightleftharpoons 2a-3	9.5	88.6	0.0018	0.086	1.63	1.63
2a-3 \rightleftharpoons 2a-4	-20.3	56.9	660	0.18	3100	3100
2a-3 \longrightarrow 5a	–	47.9	2400	–		
2a-4 \rightleftharpoons 2a-1	11.2	80.8	0.043	3.9	0.14	0.14
2b^f						
2b-1 \rightleftharpoons 2b-2	6.7	63.1	54	800	0.50 (15)	0.50 (15)
2b-2 \rightleftharpoons 2b-3	-8.7	86.0	0.0052	0.00016		
2b-3 \rightleftharpoons 2b-4	-13.0	63.2	51	0.27	75 (69)	75 (69)
2b-3 \longrightarrow 11	–	65.0	25	–		
2b-4 \rightleftharpoons 2b-1	15.0	91.6	0.00055	0.23	0.10 (16)	0.10 (16)
2b-4 \longrightarrow 6b	–	82.2	0.024	–		

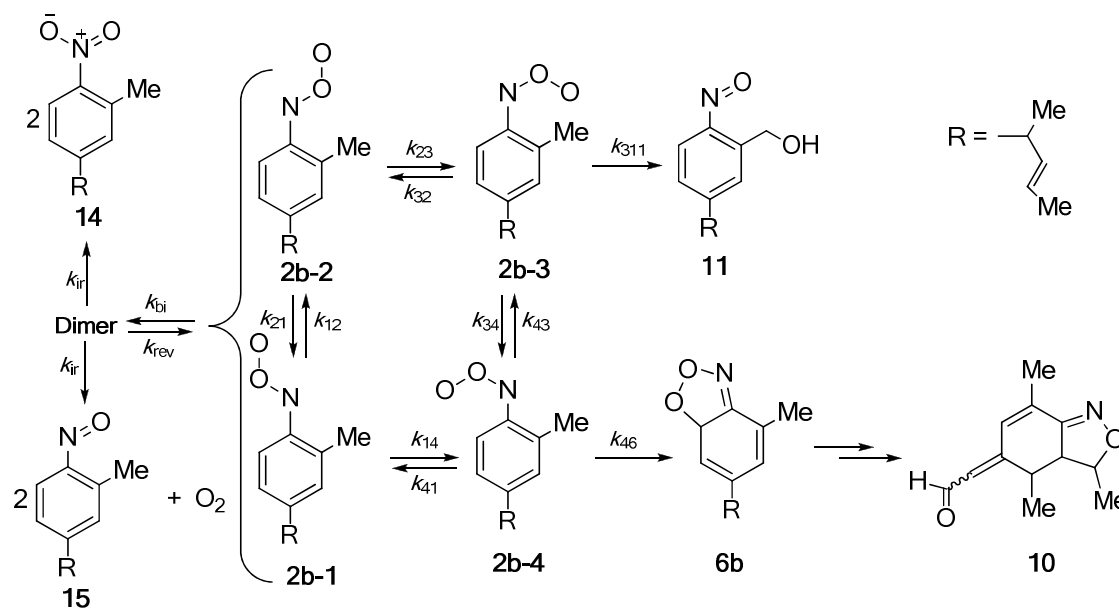
^aRelative stability of the isomers (ΔG°), Gibbs activation energy (ΔG^\ddagger) in kJ/mol, rate constants in s⁻¹ (295 K). Calculation by M06-L/6-311+G(d, p) + IEFPCM approximation. ^bIndices “+” and “-” correspond to direct and reverse reaction, respectively. ^cCalculated effective rate constant for each isomer; in the case of **2b-1** and **2b-2** k_{eff} corresponds to their joint consumption. ^dYields of corresponding products in % for nitroso oxide **2b** are given in brackets. ^eExperimental values of k_{eff} . ^fRate constants $k_{\text{bi}} = 1.0 \times 10^6 \text{ M}^{-1}\text{s}^{-1}$, $k_{\text{rev}} = 2.4 \text{ s}^{-1}$, $k_{\text{ir}} = 36 \text{ s}^{-1}$ (Scheme 8).

In general, the kinetic modeling of Scheme 7 qualitatively and quantitatively describes the observed experimental regularities. It should be noted that the Gibbs free energies of the conformers and transition states optimized during this modeling differed slightly from the G° values obtained by the DFT-calculations. The maximal discrepancy was observed for the cis isomers of **2a**, the optimized Gibbs energies of which were decreased by 7.6 (**2a-3**) and 5.3 (**2a-4**) kJ/mol. Apparently, the results of the DFT calculations somewhat underestimate the stability of the cis conformers, perhaps because a specific solvation of the polar molecule of nitroso oxide **2a** by acetonitrile is ignored.

The case of 2b. Nitroso oxide **2b** exhibited a greater variety of chemical transformations shown in Scheme 8. Therefore, the system of eight ODEs contained thirteen elementary stages including eight stages of conformational transitions between the isomers of **2b**, two stages of irreversible transformation of the cis isomers **2b-3** and **2b-4**, and three elementary stages which describe the bimolecular decay of the trans forms of **2b** according to Scheme 5. To simplify the mathematical model, the bimolecular reaction was described by the cross-reaction **2b-1** + **2b-2**, and the accumulation of products **14** and **15** was considered in the sum as a result of one

transformation. As the initial conditions for the ODE system solution, the equimolar ratio of the isomers was used.

Scheme 8. Transformations of the Conformers of Nitroso Oxide **2b**



The optimization was performed by varying the G° values of all kinetically independent species which were determined by the DFT calculations. The rate constants k_{bi} (the bimolecular decay), k_{rev} (the reversible consumption of the nitroso oxide dimer), and k_{ir} (the irreversible transformation of the dimer) were three additional optimization parameters which modeled the recombination of the trans isomers of **2b**. The condition for the convergence of a mathematical model with experiment was the coincidence of the effective rate constants of the isomers consumption (See above) as well as the equality of the calculated ratio of the reaction products yields (**10:11:(14 + 15)** = 16:69:15%) and the experimental that (Table 2). The results of the mathematic modeling of the decay of nitroso oxide **2b**, namely the optimized G° values and the elementary rate constants, are shown in Table 4. It can be seen that the mathematical model describes the experiment well, i.e. correctly predicts the k_{eff} values and the products yield.

Despite the differences in the mechanism of the decay of nitroso oxides **2a** and **2b** (Schemes 7 and 8), the results of the kinetic modeling of two reactions had much in common. As was the case for **2a**, quickly, in about 20 milliseconds, the cis/syn isomer **2b-3** was consumed (Figure 1, Curve 3). The effective rate constant of the **2b-3** consumption is the sum of two elementary constants ($k_{eff(cis/syn)} \approx k_{311} + k_{34}$), which correspond to the accumulation of product **11** (33%) and conformational transformation into **2b-4** (67%). The accumulation of the cis/anti isomer **2b-4** via the transformation of the trans isomers occurred within about 1.3 sec. The trans forms of **2b** were consumed in the parallel process, namely the conformational transformation into the

cis/anti isomer and the recombination which led to the effective first order with respect to the concentration of the trans isomers (Figure 1b, Curve 2). After 7–8 sec only the cis/anti isomer **2b-4** remained in the system (Figure 1b, Curve 1), the concentrations of the other isomers were too small for spectrophotometric detection. The effective rate constant of the **2b-4** consumption can be represented as $k_{\text{eff(cis/anti)}} \approx k_{46} + k_{43} \cdot k_{311} / (k_{311} + k_{34})$, where the first and second terms describing the accumulation of products **10** and **11**, respectively. The percentage ratio of the rates of two parallel processes is about 20% (**10**) and 80% (**11**), which explains the preferential formation of nitrosobenzyl alcohol **11** (Table 2). Interesting to note that at the initial stage of the reaction only 9% of the product **11** was formed directly from the cis/syn isomer **2b-3**. The remaining 60% was accumulated during all process of **2b** decay according to the scheme: **2b-4** → **2b-3** → **11**.

The temperature dependence of the ratio of the yields of the products of flash photolysis of azide **1b** in the presence of oxygen testifies that when increasing the temperature from 293 to 333 K, the share of benzisoxazole **10**, which was product of the irreversible transformation of the cis/anti isomer of nitroso oxide **2b**, significantly increased (Table 2). This is explained by the higher activation energy of this channel in comparison with the formation of nitrosobenzyl alcohol **11** from the cis/syn isomer (Table 4). At that, the total yield of the products of the nitroso oxides recombination was only slightly reduced (Table 2), since this reaction does not require large energy expenditures. Therefore, with decreasing temperature to 251 K, its share grew, which was reflected in the percentage ratio of the products of the uni- and bimolecular channels of nitroso oxide **2b** consumption (Table 4).

A complication of the kinetic scheme in the case of **2b** in comparison with **2a** led to an increase in the deviations of the G° optimal values from the initial ones obtained by the DFT calculations. The maximal reduction of the Gibbs free energy was again observed for the cis isomers: 17.5 (**2b-3**) and 15.3 (**2b-4**) kJ/mol (on the supposed reasons for these deviations – See above). The maximal positive deviation of the G° from the initial value (15.1 kJ/mol) was found for the transition state of the conformational transition between the cis isomers. The detailed description of the mathematic modeling of the nitroso oxides decay process is given in Supporting Information.

The results of the mathematic modeling testify that the conformational transformations of nitroso oxides **2a** and **2b** make a significant contribution to the kinetic regularities of their consumption with the formation of the final products. Therefore, the rate constant of the transformation of the cis/syn form of nitroso oxide **2a** to form the bicycle **5a** (Scheme 7) is $2.4 \cdot 10^3 \text{ s}^{-1}$ that is 1.4 times smaller than the effective rate constant of this intermediate

consumption (Table 4). An even more illustrative example is the formation of the products **10** and **11** from the *cis* form of nitroso oxide **2b** (Scheme 8): the rate constants of these transformations are 0.024 and 25 s⁻¹, respectively, which are 4 and 3 times less, respectively, than the rate constants of the decay of **2b-4** (0.10 s⁻¹) and **2b-3** (75 s⁻¹) which were found experimentally (Table 4). In addition, the bimolecular decay of the *trans* isomers of nitroso oxide **2b** complicated their conformational transformations was described by the effective first order with the rate constant of 0.50 s⁻¹.

CONCLUSION

Thus, in this work, the comprehensive study of the mechanism of the photooxidation of aromatic azides **1a** and **1b** containing the methoxy or methyl substituent at the *ortho* position was performed. The kinetic regularities of the decay of four isomeric forms of corresponding nitroso oxides **2a** and **2b** have been investigated and the quantum-chemical and kinetic modeling of this reaction was carried out. Analysis of the obtained results together with data on the composition of the products of the azides photooxidation allowed a holistic picture to be obtained, from which it follows that the conformational transitions in *ortho*-substituted aromatic nitroso oxides significantly affect the reactivity and chemical transformations of these species.

EXPERIMENTAL SECTION

HPLC grade acetonitrile (Cryochrom) were used without further purification. 2,4-Dimethoxyphenyl azide (**1a**) was synthesized from 2,4-dimethoxyaniline using the method described for phenyl azide.³⁰

1D and 2D NMR spectra were recorded at 298 K on a Bruker *Avance III* 500 MHz instrument with PABBO X{¹H} direct detection probe in deuterated acetonitrile (Cambridge Isotope Laboratories, Inc., degree of deuteration 99.8%). Chemical shifts for carbon and proton are reported in parts per million (ppm) referenced to 0.0 ppm of TMS as the internal standard.

The ¹H NMR spectra were acquired with a spectral width of 5.6 kHz and 32k data points and 8 scans, providing a digital resolution of ca. 0.5 Hz (¹H 90° pulse width = 11.5 μs). For ¹³C{¹H} NMR spectra (WALTZ-16), a spectral width of 29.7 kHz was used with 64k data points and required quantity of scans (¹³C 90° pulse width = 9.7 μs). Gradient selected {¹H, ¹³C} HSQC spectra were recorded using the Bruker pulse sequence library. These data were collected with 4096 × 512 data points with 2 scans for each increment. The delay d4 was set to 1.72 ms. Gradient selected {¹H, ¹³C} HMBC spectra were collected with 4096 × 512 data points with 4 scans for each increment. The delay d6 was set to 71.4 ms. Spectral widths of 6.0 and 29.7 kHz were used in the *F2* (¹H) and *F1* (¹³C) domains, respectively. {¹H, ¹³C} HSQC and HMBC data were processed using a sine window in the *F2* and *F1* dimensions. {¹H, ¹H} gs-COSY data were

collected with $4K \times 512$ data points with 2 scans for each increment. For the $\{^1H, ^1H\}$ NOESY NMR experiments, the solution was degassed to remove any dissolved oxygen. The following parameters and procedures are commonly employed: spectral width 6.0 kHz, 4K data matrix and 256 time increments of 2 transients each, mixing time 0.5 s. Fourier transformations were carried out with zero-filling using the shifted sine-bell apodization function in both dimensions.

The following abbreviations (or combinations thereof) were used to explain multiplicities: s = singlet, d = doublet, t = triplet, q = quartet, m = multiplet, br = broad. Coupling constants, J, were reported in Hertz unit (Hz).

UV-vis spectra were recorded on a Shimadzu UV-365 spectrometer.

The atmospheric pressure chemical ionization mass spectra (APCI-MS) were obtained on a HPLC mass-spectrometer LCMS-2010EV (Shimadzu) (direct syringe sample inlet, sample solution was in acetonitrile, mobile phase was acetonitrile/water (85:15)) in positive and negative ions mode at the corona discharge needle ionizing electrode potential of 4.5 and -3.5 kV, respectively. The mobile phase flow rate was 0.1 mL/min. The temperature and voltage of the interface capillary was 250 °C and 5 – (-5) V, respectively. The nebulizer gas (nitrogen) flow rate was 2.5 L/min. The temperature and voltage of the curved desolvation line was 250 °C and 5 – (-5) V, respectively, heater temperature was 200 °C.

High resolution mass spectra were recorded on a mass spectrometer MALDI-TOF Autoflex III (Bruker, Germany) with sinapic acid as a matrix. Samples of compounds were prepared by the “dried droplet” method (1:10).

HPLC analysis was carried out on an YL9100 liquid chromatograph equipped with a two-wave UV–Vis detector. The reverse-phase analytical column was a ProteCol C18 GP125 4.6×250 mm (SGE), the mobile phase was acetonitrile–water (92:8 or 50:50), the flow rate of mobile phase was 1 mL/min, and the column was operated at room temperature. A Reprosil-Pur C18-AQ 10×250 mm column (Dr. Maisch GmbH) was used for preparative separation of the reaction mixtures. The mobile phase was acetonitrile.

Kinetic Experiments. A flash photolysis system of known design¹⁶ was used for the kinetic experiments. The photolytic source was an IFP 5000-2 lamp; the maximum pulse energy was 400 J at $U = 5$ kV, $C = 32 \mu F$; ~90% light energy was emitted in 50 μs . The reactor was a quartz cell with an optical path length $l = 10$ cm, inner diameter of ~1 cm and volume of ~8 mL. The flash photolysis of 2.5×10^{-4} M azides **1** solutions saturated with oxygen was performed with filtered light (UFS-2 light filter; transmittance range $\lambda = 270\text{--}380$ nm).

Synthesis of 2-methyl-4-[(2E)-1-methylbut-2-en-1-yl]aniline. 26.5 g (0.25 mol) of *o*-toluidine, 17.6 g (0.26 mol) of piperylene, 7.5 g (0.056 mol) of $AlCl_3$, and 22 mL of hexane was

placed into a rotating stainless steel autoclave. The autoclave was heated at 130°C for 4 hours, and then cooled. The reaction mixture was neutralized with a 30% NaOH solution in water. The organic layer was extracted with *tert*-buthyl-methylether and dried over KOH. The solvent was evaporated; the residue was distilled under vacuum. The fraction boiling at 145–150°C (10 mmHg) was 2-methyl-4-[(2*E*)-1-methylbut-2-en-1-yl]aniline which was obtained as a yellow liquid in a yield of 14.6 g (29%). ¹H NMR (CDCl₃, 500 MHz): δ_H 6.95 (1H, d, *J* = 2.0 Hz, H3); 6.94 (1H, dd, *J* = 8.5, 2.0 Hz, H5); 6.67 (1H, d, *J* = 8.5 Hz, H6); 5.65 (1H, ddq, *J* = 15.2, 6.7, 1.1 Hz, H9); 5.49 (1H, dqd, *J* = 15.2, 6.7, 1.1 Hz, H10); 3.36 (1H, m, H8); 2.21 (3H, s, H7); 1.73 (dd, 3H, *J* = 6.0, 1.1 Hz, H11); 1.36 (3H, d, *J* = 6.7 Hz, H12). ¹³C NMR (CDCl₃, 125 MHz): δ_C 142.5 (s, C4), 137.0 (d, C9), 136.7 (s, C2), 129.1 (d, C3), 125.4 (d, C5), 122.8 (d, C10), 115.1 (d, C6), 41.5 (d, C8), 21.6 (q, C12), 17.9 (q, C11), 17.4 (q, C7).

2-Methyl-4-[(2*E*)-1-methylbut-2-en-1-yl]phenyl azide (1b**)** was synthesized from 2-methyl-4-[(2*E*)-1-methylbut-2-en-1-yl]aniline via the procedure described in the literature for trans-1-(*o*-azidophenyl)-1-pentene.³¹ **1b** was obtained as a yellow liquid. ¹H NMR (CDCl₃, 500 MHz): δ_H 7.09 (1H, dd, *J* = 8.5, 2.0 Hz, H5); 7.06 (1H, d, *J* = 8.5 Hz, H6); 7.03 (1H, d, *J* = 2.0 Hz, H3), 5.60 (1H, ddq, *J* = 15.2, 6.7, 1.1 Hz, H9); 3.38 (1H, m, H8); 2.22 (3H, s, H7); 1.71 (3H, dd, *J* = 6.0, 1.1 Hz, H11); 1.34 (3H, d, *J* = 6.7, H12). ¹³C NMR (CDCl₃, 125 MHz): δ_C 143.0 (s, C4), 136.1 (d, C9), 136.0 (s, C4), 130.0 (d, C3), 125.8 (d, C5), 123.8 (d, C10), 41.8 (d, C8), 21.5 (q, C12), 17.9 (q, C11).

Photooxidation of azide 1a. Azide **1a** (7.3 mg, 0.041 mmol) was dissolved in 60 mL of acetonitrile and placed in a thermostatically controlled (293 K) reactor. To saturate the solution with oxygen, O₂ was bubbled through it for 5 min. The resulting solution was further purged with oxygen and irradiated by means of a xenon lamp through SS-5 filter (360–500 nm) until the starting material had disappeared. The reaction mixture was concentrated to about 0.5 mL and separated chromatographically. (2*Z*,4*E*)-2-methoxy-6-oxohepta-2,4-dienenitrile oxide (**7a**) was isolated as a yellow oil in an amount of 7.0 mg (93%): ¹H NMR (CD₃CN, 500 MHz): δ_H 7.90 (1H, d, *J* = 11.4 Hz, H2), 5.84 (1H, dd, *J* = 11.4, 1.4 Hz, H3), 5.35 (1H, d, *J* = 1.4 Hz, H5), 3.79 (3H, s, H8), 3.66 (3H, s, H7). ¹³C NMR (CD₃CN, 125 MHz): δ_C 167.6 (s, C6), 164.5 (s, C4), 136.2 (d, C2), 103.9 (d, C3), 96.7 (d, C5), 57.1 (q, C7), 52.0 (q, C8), 37.3 (s, C1). APCI-MS, *m/z* (relative intensity): [M+H]⁺ 184 (100), [M-H]⁻ 182 (100), [M+H+MeCN]⁺ 225 (23), [2M+H]⁺ 367 (13). HR-MS (MALDI) calcd for C₈H₁₀NO₄ [M+H]⁺: 184.0604. Found: 184.0631. IR spectrum (KBr), ν/cm⁻¹: 2297 (C≡N). UV-Vis (MeCN): λ_{max} = 295 nm (ε = 1.0 × 10⁴ M⁻¹ cm⁻¹).

Photooxidation of the azide 1b (18.6 mg, 0.092 mmol in 180 mL acetonitrile) was carried out in a manner similar to **1a** except that its solution was irradiated with light of wavelength 270–

380 nm (UFS-2 filter). After the disappearance of the starting azide the reaction mixture was divided in half. The first part was concentrated at once and separated chromatographically to obtain the intermediate products **11** and **12** along with stable products **10**, **14**, and **15**. The second portion was stood in the dark for 72 hours and then concentrated. Chromatography of this mixture yielded the products **10**, and **13** – **15**. Compounds **11**, **13** – **15** are unstable under MALDI conditions.

{5-[(2*E*)-1-Methylbut-2-en-1-yl]-2-nitrosophenyl} methanol (**11**, 2.1 mg): ^1H NMR (CD_3CN , 500 MHz): δ_{H} 7.77 (1H, d, $J = 1.8$ Hz, H3), 7.22 (1H, dd, $J = 8.3, 1.8$ Hz, H5), 6.61 (1H, d, $J = 8.3$ Hz, H6), 5.69 (2H, s, H7), 5.64 (1H, ddq, $J = 15.2, 6.8, 1.1$ Hz, H9), 5.58 (1H, dqd, $J = 15.2, 6.1, 1.1$ Hz, H10), 3.58 (1H, m, H8), 1.67 (3H, dd, $J = 6.1, 1.1$ Hz, H11), 1.35 (3H, d, $J = 6.8$ Hz, H12). ^{13}C NMR (CD_3CN , 125 MHz): δ_{C} 164.0 (s, C2), 157.5 (s, C4), 144.2 (s, C2), 135.6 (d, C9), 128.1 (d, C3), 126.8 (d, C5), 126.0 (d, C10), 111.1 (d, C6), 60.8 (t, C7), 43.8 (d, C8), 21.4 (q, C12), 18.2 (q, C11). APCI-MS, m/z (relative intensity): $[\text{M}+\text{H}]^+$ 206 (25).

5-[(2*E*)-1-Methylbut-2-en-1-yl]-2-nitrosobenzaldehyde (**12**) was tentatively identified by molecular mass on the basis of APCI mass spectra. APCI-MS, m/z (relative intensity): $[\text{M}+\text{H}]^+$ 204 (9), $(\text{M}-\text{H})^-$ 202 (100).

(3,4,7-Trimethyl-3a,4-dihydro-2,1-benzisoxazol-5(3*H*)-ylidene)ethanal (**10**, 3.8 mg): **10a** – ^1H NMR (CD_3CN , 500 MHz): δ_{H} 10.03 (1H, d, $J = 7.8$ Hz, H12), 6.34 (1H, s, H6), 5.87 (1H, d, $J = 7.8$ Hz, H11), 4.53 (1H, dq, $J = 12.7, 6.2$ Hz, H3), 3.91 (1H, m, $J = 6.7$ Hz, H4), 3.16 (1H, dd, $J = 12.7, 6.7$ Hz, H3a), 2.07 (3H, s, H10), 1.45 (3H, d, $J = 6.2$ Hz, H8), 1.10 (3H, d, $J = 6.7$ Hz, H9). ^{13}C NMR (CD_3CN , 125 MHz): δ_{C} 191.8 (d, C12), 160.2 (s, C5), 158.0 (s, C7a), 134.9 (s, C7), 133.4 (d, C6), 127.7 (d, C11), 80.4 (d, C3), 55.0 (d, C3a), 30.6 (d, C4), 19.0 (q, C8), 17.3 (q, C10), 16.7 (q, C9). **10b** – ^1H NMR (CD_3CN , 500 MHz): δ_{H} 10.13 (1H, d, $J = 7.9$ Hz, H12), 7.27 (1H, s, H6), 5.83 (1H, d, $J = 7.9$ Hz, H11), 4.49 (1H, dq, $J = 12.8, 6.2$ Hz, H3), 3.18 (1H, dd, $J = 12.8, 6.8$ Hz, H3a), 2.90 (1H, m, H4), 2.11 (3H, s, H10), 1.44 (3H, d, $J = 6.2$ Hz, H8), 1.04 (3H, d, $J = 6.7$ Hz, H9). ^{13}C NMR (CD_3CN , 125 MHz): δ_{C} 191.8 (d, C12), 159.4 (s, C5), 158.0 (s, C7a), 134.5 (s, C7), 126.9 (d, C11), 126.2 (d, C6), 80.5 (d, C3), 55.1 (d, C3a), 38.2 (d, C4), 18.9 (q, C8), 17.5 (q, C10), 16.4 (q, C9). APCI-MS, m/z (relative intensity): $[\text{M}+\text{H}]^+$ 206 (93), $[\text{M}-\text{H}]^-$ 204 (67). HR-MS (MALDI) calcd for $\text{C}_{12}\text{H}_{16}\text{NO}_2$ $[\text{M}+\text{H}]^+$: 206.1176. Found: 206.1050. UV-Vis (MeCN): $\lambda_{\text{max}} = 315$ nm ($\epsilon = 1.0 \times 10^4 \text{ M}^{-1} \text{ cm}^{-1}$).

(*Z*)-1,2-Bis(2-formyl-4-((2*E*)-1-methylbut-2-en-1-yl)phenyl)diazene 1-oxide (**13**, 2.0 mg): ^1H NMR (CD_3CN , 500 MHz): δ_{H} 10.33 (1H, s, H7'), 10.32 (1H, s, H7), 8.05 (1H, d, $J = 8.2$ Hz, H6), 7.98 (1H, d, $J = 8.2$ Hz, H6'), 7.84 (1H, d, $J = 2.1$ Hz, H3'), 7.75 (1H, d, $J_{3-5} = 2.0$ Hz, H3), 7.67 (1H, dd, $J = 8.2, 2.1$ Hz, H5), 7.66 (1H, dd, $J = 8.2, 2.1$ Hz, H5'), 5.67 (2H, m, H9 and H9'),

5.59 (1H, dqd, $J = 15.2, 6.0, 1.1$ Hz, H10), 5.56 (1H, dqd, $J = 15.2, 6.0, 1.1$ Hz, H10'), 3.65 (1H, m, H8), 3.60 (1H, m, H8'), 1.68 (6H, both dd, $J = 6.0, 1.1$ Hz, H11 and H11'), 1.38 (3H, d, $J = 6.7$ Hz, H12), 1.37 (3H, d, $J = 6.7$ Hz, H12'). ^{13}C NMR (CD_3CN , 125 MHz): δ_{C} 191.9 (d, C7'), 190.7 (d, C7), 152.2 (s, C4), 149.1 (s, C4'), 148.4 (s, C1), 143.6 (s, C1'), 136.2 (d, C9'), 135.8 (d, C9), 134.3 (d, C5'), 133.6 (d, C5), 131.7 (s, C2), 131.1 (s, C2'), 129.1 (d, C3'), 128.9 (d, C3), 126.3 (d, C10), 125.8 (d, C10'), 125.3 (d, C6), 123.6 (d, C6'), 42.87 (d, C8'), 42.85 (d, C8), 21.59 (q, C12), 21.58 (q, C12'), 18.13 (q, C11), 18.12 (q, C11'). APCI-MS, m/z (relative intensity): $[\text{M}+\text{H}]^+$ 391 (100), $[\text{M}-\text{H}]^-$ 389 (47). UV-Vis (MeCN): $\lambda_{\text{max}} = 330$ nm ($\epsilon = 1.0 \times 10^4 \text{ M}^{-1} \text{ cm}^{-1}$).

2-Methyl-4-[(2*E*)-1-methylbut-2-en-1-yl]-1-nitrobenzene (**14**, 4.9 mg): ^1H NMR (CD_3CN , 500 MHz): δ_{H} 7.91 (1H, d, $J = 8.5$ Hz, H6), 7.28 (1H, d, $J = 2.0$ Hz, H3), 7.24 (1H, dd, $J = 8.5, 2.0$ Hz, H5), 5.61 (1H, ddq, $J = 15.2, 6.7, 1.1$ Hz, H9), 5.54 (1H, dqd, $J = 15.2, 6.0, 1.1$ Hz, H10), 3.50 (1H, m, H8), 2.55 (3H, s, H7), 1.66 (3H, dd, $J = 6.0, 1.1$ Hz, H11), 1.32 (3H, d, $J = 6.7$ Hz, H12). ^{13}C NMR (CD_3CN , 125 MHz): δ_{C} 153.7 (s, C4), 148.4 (s, C1), 135.9 (d, C9), 134.8 (s, C2), 132.5 (d, C3), 126.7 (d, C5), 125.9 (d, C6), 125.8 (d, C10), 43.0 (d, C8), 21.6 (q, C12), 20.7 (q, C7), 18.1 (q, C11). APCI-MS, m/z (relative intensity): $[\text{M}+\text{H}]^+$ 206 (78), $[\text{M}-\text{H}]^-$ 204 (67). UV-Vis (MeCN): $\lambda_{\text{max}} = 265$ nm ($\epsilon = 9.3 \times 10^3 \text{ M}^{-1} \text{ cm}^{-1}$).

2-Methyl-4-[(2*E*)-1-methylbut-2-en-1-yl]-1-nitrosobenzene (**15**, 2.2 mg): ^1H NMR (CD_3CN , 500 MHz): δ_{H} 7.47 (1H, d, $J = 2.0$ Hz, H3), 7.07 (1H, dd, $J = 8.5$ Hz, H5), 6.27 (1H, d, $J = 8.5$ Hz, H6), 5.62 (1H, ddq, $J = 15.2, 6.7, 1.1$ Hz, H9), 5.55 (1H, dqd, $J = 15.2, 6.0, 1.1$ Hz, H10), 3.49 (1H, m, H8), 3.28 (3H, s, H7), 1.66 (3H, dd, $J = 6.0, 1.1$ Hz, H11), 1.33 (3H, d, $J = 6.7$ Hz, H12). ^{13}C NMR (CD_3CN , 125 MHz): δ_{C} 166.1 (s, C1), 157.4 (s, C4), 143.9 (s, C2), 135.7 (d, C9), 132.3 (d, C3), 126.0 (d, C10), 125.7 (d, C5), 108.5 (d, C6), 43.5 (d, C8), 21.4 (q, C12), 18.1 (q, C11), 17.5 (q, C7). APCI-MS, m/z (relative intensity): $[\text{M}+\text{H}]^+$ 190 (100), $[\text{M}-\text{H}]^-$ 188 (40), $[\text{M}+\text{H}+\text{MeCN}]^+$ 231 (38). UV-Vis (MeCN): $\lambda_{\text{max}} = 320$ nm ($\epsilon = 1.2 \times 10^4 \text{ M}^{-1} \text{ cm}^{-1}$).

Methods of Calculation. The wave function of nitroso oxides has a prominent multi-configurational character; therefore, an intensive account is required for both static and dynamic electron correlation.²⁹ High-level calculations are unacceptable for aromatic nitroso oxides because of resource constraints; therefore, the use of methods of the density functional theory (DFT), namely M06-L, mPWPW91, OLYP, and HCTH, which adequately describe the structure, energetic and spectral properties of aromatic nitroso oxides, seemed to be a good alternative to the sophisticated time-consuming methods.²¹

Quantum chemical calculations were performed on the cluster supercomputer of Ufa Institute of Chemistry of the RAS using Gaussian 09, Revision C01 program package.³² Visualization of the results was performed in ChemCraft program.³³ All geometric and energy values given in the

text (unless otherwise specified) were obtained using the M06-L and mPWPW91 functionals in conjunction with the Pople basis set of triple valence splitting – 6-311+G(d,p). It was found that the wave functions of ground states and products of intramolecular reactions of nitroso oxides are stable with respect to breaking symmetry of α and β spin electronic systems, whereas transition states show some spin polarization. The calculations were carried out in an approximation of isolated molecules. The polarizable continuum model (IEFPCM) was used to account a solvent effect. The full optimization of the structures of all isomeric forms, transition states of conformational transitions and irreversible transformations of aromatic nitroso oxides under study has been carried out using the above-mentioned methods. The type of stationary points was determined by the number of negative elements in the diagonalized Hessian matrix. The correspondence of the transition states to the reagents and products was confirmed by scanning the intrinsic reaction coordinate. The relative energetic values (energies of transition states of reactions and conformational transformations, energies of conformers and heat effects of reactions) were calculated as the difference between the absolute enthalpies of the final (or transition) and initial states of a transformation under study. The absolute enthalpies were calculated as the sum of total energy, zero point vibration energy, and thermal correction for enthalpy change from zero to 298 K. The last values were obtained from the calculations of frequencies using the known equations of statistical thermodynamics.

ASSOCIATED CONTENT

SUPPORTING INFORMATION

Copies of ^1H NMR and ^{13}C NMR, IR spectra and APCI mass spectra; cartesian coordinates of the stationary points of nitroso oxides **2a** and **2b**; reaction enthalpies ΔH° , and activation enthalpies ΔH^\ddagger for the intramolecular reactions of **2a** and **2b**; kinetic modeling data of the **2a** and **2b** conformers decay. This material is available free of charge via the Internet at <http://pubs.acs.org>.

Notes

The authors declare no competing financial interest.

ACKNOWLEDGMENT

The theoretical investigations were performed and NMR and APCI mass spectra were recorded on equipment installed in the Center for Collective use “Khimiya” (Chemistry) at Ufa Institute of chemistry of the Russian Academy of Sciences.

REFERENCES

- (1) Gritsan, N. P. *Russ. Chem. Rev.* **2007**, *76*, 1139.
- (2) Sawwan, N.; Greer, A. *Chem. Rev.* **2007**, *107*, 3247.
- (3) Ishiguro, K.; Sawaki, Y. *Bull. Chem. Soc. Jpn.* **2000**, *73*, 535.
- (4) Chainikova, E. M.; Khursan, S. L.; Safiullin, R. L. In *The Chemistry of Peroxides*; Greer, A., Liebman, J. F., Eds.; John Wiley & Sons, Ltd: Chichester, UK, 2014; Vol. 3.
- (5) Brinen, J. S.; Singh, B. *J. Am. Chem. Soc.* **1971**, *93*, 6623.
- (6) Harder, T.; Wessig, P.; Bendig, J.; Stosser, R. *J. Am. Chem. Soc.* **1999**, *121*, 6580.
- (7) Inui, H.; Irisawa, M.; Oishi, S. *Chem. Lett.* **2005**, *34*, 478.
- (8) Pritchina, E. A.; Gritsan, N. P.; Bally, T. *Phys. Chem. Chem. Phys.* **2006**, *8*, 719.
- (9) Mieres-Perez, J.; Mendez-Vega, E.; Velappan, K.; Sander, W. *J. Org. Chem.* **2015**, *80*, 11926.
- (10) Talipov, M. R.; Ryzhkov, A. B.; Khursan, S. L.; Safiullin, R. L. *J. Struct. Chem.* **2006**, *47*, 1051.
- (11) Gritsan, N. P.; Pritchina, E. A. *J. Inf. Rec. Mater.* **1989**, *17*, 391.
- (12) Hiberty, P. C.; Ohanessian, G. *J. Am. Chem. Soc.* **1982**, *104*, 66.
- (13) Chainikova, E. M.; Khursan, S. L.; Safiullin, R. L. *Kinet. Catal.* **2006**, *47*, 566.
- (14) Chainikova, E. M.; Safiullin, R. L.; Spirikhin, L. V.; Abdullin, M. F. *J. Phys. Chem. A* **2012**, *116*, 8142.
- (15) Chainikova, E. M.; Pankratyev, E. Y.; Teregulova, A. N.; Gataullin, R. R.; Safiullin, R. L. *J. Phys. Chem. A* **2013**, *117*, 2728.
- (16) Chainikova, E. M.; Safiullin, R. L.; Faizrakhmanova, I. M.; Galkin, E. G. *Kinet. Catal.* **2009**, *50*, 174.
- (17) Chainikova, E.; Khursan, S.; Lobov, A.; Erastov, A.; Khalilov, L.; Mescheryakova, E.; Safiullin, R. *Tetrahedron. Lett.* **2015**, *56*, 4661.
- (18) Pritchina, E. A.; Gritsan, N. P. *J. Photochem. Photobiol. A* **1988**, *43*, 165.
- (19) Annunziata, R.; Cinquini, M.; Cozzi, F.; Gennari, C.; Raimondi, L. *J. Org. Chem.* **1987**, *52*, 4674.
- (20) Hassner, A.; Amarasekara, A. S.; Padwa, A.; Bullock, W. H. *Tetrahedron. Lett.* **1988**, *29*, 715.
- (21) Yusupova, A. R.; Safiullin, R. L.; Khursan, S. L. *J. Phys. Chem. A* **2016**, *120*, 5693.
- (22) Slayden, S. W.; Greer, A.; Liebman, J. F. In *The chemistry of hydroxylamines, oximes and hydroxamic acids*; Rappoport, Z., Liebman, J. F., Eds.; John Wiley & Sons Ltd: 2011; Vol. 2.

- (23) Denisov, E. T.; Denisova, T. G.; Pokidova, T. S. *Handbook of Free Radicals Initiators*, Wiley-Interscience: Hoboken, 2003.
- (24) Denisov, E. T.; Afanas'ev, I. B. *Oxidation and Antioxidants in Organic Chemistry and Biology*, CRC press: Boca Raton, 2005.
- (25) Sander, W.; Kirschfeld, A.; Kappert, W.; Muthusamy, S.; Kiselewsky, M. *J. Am. Chem. Soc.* **1996**, *118*, 6508.
- (26) *The Chemistry of the Nitro and Nitroso Groups*; Feuer, H., Ed.; John Wiley & Sons: New York-London-Sydney-Toronto, 1969; Vol. 1.
- (27) Sikalo, N.; Hasemann, O.; Schulz, C.; Kempf, A.; Wlokas, I. *Int. J. Chem. Kinet.* **2014**, *46*, 41.
- (28) Talipov, M. R.; Khursan, S. L.; Safiullin, R. L. *Russ. J. Phys. Chem. A* **2012**, *86*, 235.
- (29) Talipov, M. R.; Khursan, S. L.; Safiullin, R. L. *J. Phys. Chem. A* **2009**, *113*, 6468.
- (30) Lindsay, R. O.; Allen, G. F. *Organic Syntheses*; Wiley: New York, 1955; Vol. 3.
- (31) Sundberg, R. J.; Russel, H. F.; Ligon, W. V., Jr.; Lin, L.-S. *J. Org. Chem.* **1972**, *37*, 719.
- (32) Frisch, M. J.; Trucks, G. W.; Schlegel, H. B.; Scuseria, G. E.; Robb, M. A.; Cheeseman, J. R.; Scalmani, G.; Barone, V.; Mennucci, B.; Petersson, G. A.; Nakatsuji, H.; Caricato, M.; Li, X.; Hratchian, H. P.; Izmaylov, A. F.; Bloino, J.; Zheng, G.; Sonnenberg, J. L.; Hada, M.; Ehara, M.; Toyota, K.; Fukuda, R.; Hasegawa, J.; Ishida, M.; Nakajima, T.; Honda, Y.; Kitao, O.; Nakai, H.; Vreven, T.; Montgomery, J., J. A.; Peralta, J. E.; Ogliaro, F.; Bearpark, M.; Heyd, J. J.; Brothers, E.; Kudin, K. N.; Staroverov, V. N.; Kobayashi, R.; Normand, J.; Raghavachari, K.; Rendell, A.; Burant, J. C.; Iyengar, S. S.; Tomasi, J.; Cossi, M.; Rega, N.; Millam, J. M.; Klene, M.; Knox, J. E.; Cross, J. B.; Bakken, V.; Adamo, C.; Jaramillo, J.; Gomperts, R.; Stratmann, R. E.; Yazyev, O.; Austin, A. J.; Cammi, R.; Pomelli, C.; Ochterski, J. W.; Martin, R. L.; Morokuma, K.; Zakrzewski, V. G.; Voth, G. A.; Salvador, P.; Dannenberg, J. J.; Dapprich, S.; Daniels, A. D.; Farkas, Ö.; Foresman, J. B.; Ortiz, J. V.; Cioslowski, J.; Fox, D. J.; *Gaussian 09*, revision C.1; Gaussian, Inc.: Wallingford, CT, 2009.
- (33) Zhurko, G. A. *Chemcraft*, version 1.6 (Build 332); <http://www.chemcraftprog.com>.